Title: Systematic Mapping of the Monkey Inferior Colliculus Reveals Enhanced Low Frequency Sound Representation

Authors: David A. Bulkin[1], Jennifer M. Groh[1,2,3]

Affiliation:

1. Department of Neurobiology, Duke University, Durham NC

2. Department of Psychology and Neuroscience, Duke University, Durham NC

3. Center for Cognitive Neuroscience, Duke University, Durham NC

Running Head: Enhanced Low Frequency Sound Representation in the Macaque IC

Contact Information:

Address: David Bulkin, LSRC Rm B203, Duke University, Box 90999, Durham, NC 27708

Email: dave.bulkin@duke.edu -

Phone: (919) 684-6729

Fax: (919) 681-0815

Abstract (250 words)

We investigated the functional architecture of the inferior colliculus (IC) in rhesus monkeys. We systematically mapped multiunit responses to tonal stimuli and noise in the IC and surrounding tissue of six rhesus macaques, collecting data at evenly placed locations and recording non-responsive locations to define boundaries. The results show a modest tonotopically organized region (17 of 100 recording penetration locations in 4 of 6 monkeys) surrounded by a large mass of tissue that, though vigorously responsive, showed no clear topographic arrangement (68 of 100 penetration locations). Rather, most cells in these recordings responded best to frequencies at the low end of the macaque auditory range. The remaining 15 (of 100) locations exhibited auditory responses that were not sensitive to sound frequency. Potential anatomical correlates of functionally defined regions, and implications for midbrain auditory prosthetic devices are discussed.

Keywords: Auditory, topography, tonotopy, prosthetic, auditory midbrain implant

Introduction

Maps of how neural response properties vary as a function of the location within a brain structure can provide a useful bridge between neurophysiology and anatomy. Also referred to as functional architecture, such maps allow the activity of a neuron to be interpreted in light of its putative inputs and outputs. Response maps are also useful for guiding the placement of neural prosthetics (eg. (Wessberg et al. 2000)). The inferior colliculus (IC) has recently emerged as a candidate structure for such prosthetics (Colletti et al. 2007; Colletti et al. 2009; Lim and Anderson 2006; 2007; Lim et al. 2009; Lim et al. 2008), so understanding the geographical arrangement of response properties in this structure can provide guidance for implant placement.

The IC is a principal site of convergence along the auditory pathway. Virtually all ascending auditory information passes through the IC on the way to thalamus (Aitkin and Phillips 1984), and so it is an especially important locus to investigate functional maps. The tonotopic organization, or orderly progression of frequency tuning properties, has been studied in a wide variety of animals (eg. rats (Clopton and Winfield 1973; Kelly et al. 1991); cats (Aitkin et al. 1975; Merzenich and Reid 1974; Rose et al. 1963); guinea pigs (Malmierca et al. 1995); mice (Stiebler and Ehret 1985);; ferrets (Moore et al. 1983); owls (Knudsen and Konishi 1978); bats ((Casseday and Covey 1992; Miller et al. 2005; Poon et al. 1990; Zook et al. 1985)).

However, little is known about the functional map of the IC in primates. Macaques provide an excellent model for human hearing as both humans and macaques rely greatly on audition for communication, and the frequency ranges heavily overlap: approximately 30 Hz to 30 kHz for monkeys (Pfingst et al. 1975; Pfingst et al. 1978; Stebbins et al. 1966), 20 Hz to 20 kHz for humans (Moore 2008). Studies in monkeys also offer advantages not directly related to audition: monkeys are readily trained, and phenomena such as eye-movements that cannot be

studied in other mammals can be studied in monkeys (eg. (Groh et al. 2001; Porter et al. 2006; Zwiers et al. 2004)). Functional maps are essential to guide this work.

No detailed map of the monkey IC yet exists. Ryan and Miller (1978) recorded the auditory responses of single units along penetrations through the macaque IC, but did not collect data with uniform spacing between recordings, and primarily sampled neurons in the most central region. Zwiers and colleagues (2004) also recorded the responses of single units from the macaque IC, and noted the depth of recordings. Location in the horizontal plane was not systematically varied in this study, and the majority of recording were thought to have been taken from a similar central region as in the study by Ryan and Miller.

Accordingly we performed a systematic mapping of auditory responses throughout the midbrains of six unanesthetized rhesus monkeys. We presented a series of randomly interleaved sounds as we recorded multi-unit activity (MUA; the times of action potentials of small clusters of neurons). MUA provides an estimate of local activity, and serves as an ideal measurement as recording locations can be predefined (unlike single unit activity where fine movement of the electrode is necessary for isolating individual waveforms). We collected data in sessions in which we lowered an electrode in 0.5mm increments through the midbrain. Over sessions we varied the anterior/posterior and medial/lateral trajectory of our electrodes in 1mm increments. In this manner we formed a map of the entire region, collecting data from the IC and surrounding tissue.

In each monkey we found a large region with neurons that showed vigorous, short latency responses to auditory stimuli. In 4 of 6 monkeys we found a tonotopic area in which recording penetrations showed an orderly progression of tuning frequencies as the electrode passed through the IC. Surrounding this area was a large non-tonotopic region. In these penetrations, neurons generally showed the most powerful response to low frequencies, a bias

which has not been identified previously. Neurons in the low frequency region generally showed more transient and slower responses than those in the tonotopic area. Finally, a small subset of recordings on the periphery of the responsive area showed little or no tuning to tone frequency. We conclude that in the awake monkey, auditory neurons surrounding the central (tonotopic) area show a powerful bias toward low frequencies.

Methods

Surgical Preparation, Recording Procedures, and Inclusion Criteria

Three male and three female rhesus monkeys participated in the experiments. All procedures were approved by the Institutional Animal Care and Use Committee at Dartmouth College and Duke University, and were conducted in accordance with the principles of laboratory animal care of the National Institutes of Health (publication 86-23, revised 1985). Surgical procedures were performed using isoflurane anesthesia and aseptic techniques, as well as postoperative analgesia. The monkeys underwent an initial surgery to implant a head post for restraining the head and a scleral eye coil for monitoring eye position (Judge et al. 1980; Robinson 1963). After recovery, an additional surgery was performed to make a craniotomy and to implant a recording cylinder positioned over the left IC. The cylinder was oriented to allow electrodes to approach the IC at an angle approximately 30° from vertical in the coronal plane, i.e. proceeding from dorsolateral to ventromedial (Groh et al. 2003; Porter et al. 2007). For simplicity and convenience, we will usually refer to the affected dimensions as lateral/medial and dorsal/ventral (or above/below), despite their tilt (ie. in the axis defined by the recording chamber). The chamber contained a fixed grid of holes (Crist Instruments, Gaithersburg, MD) aligned such that electrode penetrations could be made in 1mm increments in the anterior/posterior and medial/lateral dimensions. Recordings were made using tungsten

microelectrodes (1-3 MΩ; FHC Inc, Bowdoin, ME). Multiunit clusters were selected using a window discriminator (Monkeys A,W: Plexon Inc, Dallas, TX; Monkeys E,M,C,X: Bak Electronics, Germantown, MD) and spike times were stored for off-line analysis.

The location of the IC was determined using an anatomical MRI scan in which the recording chamber and plastic grid could be visualized. Several marker electrodes were placed in the plastic grid. Images were then aligned precisely along the axis of the grid, such that recording locations could be mapped directly onto anatomical landmarks visible in MRI. Using MRI we estimated all of the borders of the IC except on the rostral aspect, where a clear definition was not visible. In each monkey we recorded from a patch around the estimated IC location, making a series of electrode penetrations through the holes in the recording grid. We lowered electrodes along the dorsolateral/ventromedial axis of the IC (established by the placement of the recording cylinder) and recorded from multiunit clusters every 0.5mm along the trajectory of the penetration. Figure 1 shows MR images spanning the recorded region of monkey A, the most thoroughly sampled monkey in our data set. The images are spaced in 1mm increments, such that each image corresponds to a row of recordings in the anterior/posterior aspect of the recording grid. The locations of recording trajectories (medial/lateral aspect of the recording grid) have been plotted with red lines. We began and ended recording sessions at depths above and below the putative IC to ensure that the entire structure was covered, but limited our analysis to locations between the borders measured from the MRI scans, +/- 1.5 mm. This constraint is indicated with green lines of figure 1.

Some recording grid locations were sampled multiple times on different days, to verify that the results for those holes were reproducible across sessions. Table 1 lists both raw totals and totals with duplicate penetrations excluded. Duplicate penetrations were also excluded for analyses related to the proportion of IC tissue that shows a particular property. Such cases are

specifically noted as they arise. Unless otherwise mentioned, analyses were conducted on the complete data set without excluding the duplicates.

Data were analyzed offline to determine which sites along a penetration showed auditory responses. The times of action potentials were binned in 1ms windows aligned on stimulus onset to form a peri-stimulus time histogram (PSTH) for all auditory stimuli presented. The PSTH was then smoothed using a 5ms moving average. A site was marked as auditory if the smoothed PSTH exceeded 3 standard deviations above baseline for 10 consecutive milliseconds in a 50ms window following stimulus onset. We further restricted analysis to penetrations that contained 3 or more responsive sites. Finally, as noted above, we excluded responsive sites that were more than 1.5mm shallower or deeper than anatomical estimates gathered from MRI (borders for Monkey A indicated on Figure 1). The objective marking of auditory stretches through the IC corresponded well with subjective markings based on inspection of PSTHs and tuning curves, and locations agreed well with anatomical indications from MRI and histological reconstruction in monkeys W and X detailed below.

We tested a subset of sites in monkey A, notably those in the rostral-most penetrations, with microstimulation to rule out that they were in the superior colliculus (SC). The SC is an oculomotor structure rostral and dorsal to the IC, and it exhibits auditory responsiveness (Jay and Sparks 1984; Populin et al. 2004). However, the SC's auditory activity is quite weak when the animal is not engaged in a task involving saccades to auditory stimuli (Jay and Sparks, 1987a,b). Our monkeys were not performing an auditory saccade task, so we did not expect to see, nor did we observe, strong auditory responses in the SC. Occasionally, sites with weak auditory responses in the vicinity of the SC were observed, but these were generally excluded from our IC sample by either the MRI or because firing rate changes did not meet the response threshold described above. Stimulation allowed us to confirm that these exclusion criteria were adequate: only 2 of 51 sites included for analysis of auditory characteristics showed saccades

following stimulation onset, confirming that the inclusion criteria successfully excluded the SC. Instead, when saccades were observed, they were evoked at sites dorsal to the IC, consistent with some penetrations passing through the intermediate and deep layers of the SC on the way to the underlying IC.

Stimulus Presentation

Experiments were conducted in complete darkness in a single-walled IAC sound isolation booth. Echo-absorbent material lined the walls and ceiling (3-in. Sonex Painted One acoustic foam), as well as the floor (carpet). Auditory stimuli consisted of tones of 16 frequencies ranging from 0.4 to 12kHz (approximately ¼ octave increments), as well as broadband noise (spectrum ranging from 0.5 to 18kHz). In Monkey W we recorded several sites which included the presentation of 8 additional frequencies ranging from 0.1 to 0.33kHz. In Monkeys A and W sounds were presented for 200ms, in all other recordings sounds were presented for 500ms. All sounds were initiated with a 10ms on ramp. At each recording site, 200 total trials (more in cases where we presented additional frequencies) were presented in a randomly interleaved fashion (about 12 trials per stimulus).

Sounds were generally presented using loudspeakers (Audax Model TWO25V2, or Bose Acoustimas cube speakers) located 90 degrees contralateral to the recording chamber and 57 inches from the subject's head. In all monkeys sounds were presented at 50dB SPL. Sound levels were calibrated to within 1dB of the target amplitude using a sound meter (Brüel & Kjær, model 2237 with model 4137 condenser microphone; A-weighted) placed at the position that the monkey's head would occupy in the experiment. Sound spectra are shown in supplementary

figure 9. Eye position was monitored throughout the experiment and the monkey was woken if drifting eye movements characteristic of sleep were observed. In monkeys A, W, E and M an unrelated non-auditory task was run at some recording sites as part of a separate experiment, not described here. These trials were run in separate blocks after collecting frequency information at a given depth.

Data analysis

Frequency tuning: To characterize frequency tuning, we counted spikes in a 200ms window following sound onset and compared it to a 200ms baseline period before the sound. We computed this response for each of the different stimulus frequencies, i.e. an (isointensity) frequency response curve. Gaussian curves were then fit to the responses as a function of the logarithm of the stimulus frequency. Fitting of Gaussian functions was performed in Matlab (Mathworks, Natick MA) using the "fit" function. Gaussian fits were constrained to have peaks in the range of frequencies tested. The best frequency (BF) was labeled as the frequency corresponding to the peak of the Gaussian curve, provided the Gaussian successfully described the data (F-test, $p<0.05$). Sites for which Gaussians did not fit showed no apparent tuning by inspection, and were included only for analysis of non-tuning related features. Gaussian defined BFs were similar to the frequency evoking the maximum response (an alternative measure of BF), but allowed us to take into consideration the responses of neighboring frequencies in estimating BF. Penetrations were classified as **tuned** if 3 or more sites were fit by Gaussian functions. Penetrations with fewer were classified as **untuned**. Such penetrations could include either sites not very responsive to tones or responsive to tones but insensitive to their frequency.

Tuned penetrations were tested for the presence of a **tonotopic** progression by relating the BF to depth with a linear regression. Because each BF measurement reflected ~200 trials, treating them as a single data point in the regression would cause an underestimate of the true confidence intervals around the regression slope. Accordingly, we performed a Monte Carlo simulation. For each penetration, we ran 100 iterations in which we randomly selected 75% of the trials for each multiunit cluster and fit Gaussian tuning curves to each of the data subsets. We then fit regression lines to log(BF) vs. depth for each of iterations. This process allowed us to create a 95% confidence interval for the slopes of regression lines without making any assumptions about the distribution of slopes. Based on previous studies in monkeys and other mammals, we expected BF to increase with depth (eg. in monkey: (FitzPatrick 1975; Ryan and Miller 1978; Zwiers et al. 2004)). We defined tonotopic penetrations as those in which 95% of slopes from the Monte Carlo simulation were positive. Only significant Gaussian fits were used in the simulation, and on some iterations there were insufficient fits to perform a regression. Only penetrations which had at least 75 successful iterations were included. This analysis matched our subjective marking of tonotopy by visual inspection of the responses as a function of sound frequency over the course of a penetration.

Temporal profile: To characterize the temporal profile of the response, we measured the firing rate in two windows. We defined the sustained response as the average firing rate in a period 100 to 200 ms following stimulus onset and the transient response as the average firing rate in a 20ms period centered on the peak of the PSTH over the first 50ms following stimulus onset. Firing rates in both windows were converted to z-scores relative to the mean and standard deviation of the firing rate during a baseline period (0 to 200 ms prior to sound onset).

To compare the response profile across recordings, we created a response profile index (RPI):

$$RPI=(transient-sustained)/transient+sustained)$$

This index provides a metric for how sustained a response is: sites which exhibit almost no sustained responses produce RPI values around 1, whereas sites with sustained responses similar in magnitude to transient responses produce RPI values near 0. (The RPI could exceed 1 if an excitatory transient was followed by an inhibitory sustained component).

Latency: Latency was defined as the time (with respect to stimulus onset) that the PSTH exceeded 3 standard deviations of baseline. Because stimuli were generally presented from loudspeakers, latency included the time it took for the sound to travel to the ear, about 4ms, (i.e. to convert to latency from the arrival of the sound at the ear to the neural response, subtract ~4 ms).

Histology

In monkeys W and X, at the conclusion of recordings, an electrolytic lesion was made along a central penetration. The animal was perfused, and the brain was fixed with formalin. In monkey W the brain was sliced in 60 μm coronal sections stained with cytochrome oxidase, in monkey X 50 μm sections were cut and stained with cresyl violet. The histological analysis of monkey W was performed by the Cant laboratory at Duke University and that of monkey X was performed by the Winer laboratory at UC Berkeley.

Sources of error in determining recording locations

Certain sources of error affected the reliability of our estimate of recording location. The most reliable measurement is the depth within a penetration. The accuracy of this measurement is

on the order of microns – i.e. the accuracy of our microdrive (Narishige, model MO-951). The overall depth is estimated less accurately. There are two sources of error here. The first is that a paint mark is placed at a measured position on each electrode before they are placed in the microdrive. The mark is then aligned with the scale on the microdrive. The precision of this paint mark and its alignment is on the order of about 1 mm or so. The second issue is the head implant itself, which can gradually lift over time as tissue grows beneath the acrylic, moving the cylinder slightly. These changes are small and slow. However the more time that elapses, the less fidelity there is between the overall depth estimate and that predicted from the MRI scan (which was typically done once before the mapping began). It was to allow for these sources of error that we included a 1.5 mm buffer zone above and below the estimated depth of the IC. Overall, the depth measurements of responsive sites corresponded well to the predicted depth of the IC, suggesting that these sources of error were largely variable and not systematic errors. As noted above, a number of penetration locations were sampled repeatedly, and results were qualitatively consistent across multiple penetrations, providing further evidence that changes due to shifting of the implant were minimal.

Potential error in the AP and ML dimensions arises due to head cap shifting, as mentioned above, and also electrode bending as the IC is approached. The IC is about 5 cm below the top of our recording grid. Part of this distance was traversed with the electrode in a rigid guide tube, but at least the last cm was traversed by the electrode alone. The tungsten electrodes could bend as the approached the IC, or could potentially slip alongside it especially on the lateral aspect. This source of error probably accounts for less than 1 mm variation in the precise AP or ML position of electrode on repeated penetrations through the same grid location.

Sources of error in MRI reconstruction relate to the quality of the image and voxel size, the thickness of coronal slices ranged between 0.5 mm and 1 mm, the other two dimensions were fixed at 0.5 mm across scans. The visibility of morphological features of the IC on the

scan, and our ability to estimate the position of the cylinder and electrodes on the scan also influence the accuracy with which recording locations could be reconstructed. Reconstructing the borders of the IC via MRI scan using similar techniques has been estimated to be accurate to the nearest 1 mm (Kalwani et al. 2009).

Results

We systematically mapped the IC of 6 monkeys by recording multi-unit activity along electrode penetrations through the structure while presenting a series of auditory stimuli. We classified penetrations based on responsiveness to tones: penetrations showing auditory responses were classified as either tuned or untuned, and tuned penetrations were further classified based on whether or not they showed a tonotopic progression (Table 1).

Figure 2 shows an example tuned, non-tonotopic, penetration, the type we observed most frequently (in 68 of 100 auditory-responsive penetrations, numbers from reduced data set with one penetration per grid hole). The responses of each trial (the average firing rate in a 200 ms period following stimulus onset, normalized to baseline) are plotted against the stimulus. The recordings are plotted in the order they were taken, with the shallowest recordings at the top and the deepest recordings at the bottom. Only the responsive recordings are shown, though nonresponsive recordings flanked the auditory area above and below. Gaussian fits to the data, used below to summarize tuning, are overlaid. The recordings at each of the depths showed clear auditory responses (an increase in the height of the PSTH (shown in the inset on each tuning curve following stimulus onset) that were strongly tuned to low frequencies (around 650Hz). At the deepest recording, only a small response to tones is seen, though this site responded well to broadband white noise.

Tonotopic penetrations were more rare, found in 17 of 100 auditory-responsive penetration locations). Figure 3 shows data from an example tonotopic penetration in the same format as figure 2. Sites along this penetration, in contrast to the non-tonotopic example, exhibit an orderly increase in BF. The first responsive recording in this penetration showed only a small response and no clear tuning (this site responded best to white noise). The second site was tuned to the lowest frequency sounds we presented, deeper sites showed maximal responses

303 to progressively higher frequencies. To objectively determine the tonotopicity of penetrations we
304 performed a Monte Carlo simulation, calculating regressions on the slope of BF over depth on
305 randomly selected subsets of the data at each site (see methods for details). The inset shows a
306 histogram of the slopes of regressions over the simulation for this penetration. Sites were
307 marked as tonotopic if 95% of the slopes were positive (in this example, all iterations showed
308 positive slopes in contrast to the example in figure 2 which showed no such trend; note the very
309 different x-axis scales for these two insets).

310 Figure 4 shows the responses of an untuned recording. Untuned penetrations (defined
311 as having less than three sites showing tuned responses) were uncommon and only found at
312 the most peripheral sites sampled. Lack of tuning occurred when sites responded to tones
313 without clear modulation based on tone frequency, or when the sites responded only to
314 presentations of broadband white noise. Most of the untuned recordings in our sample showed
315 some response to tones (120 of 185 sites, t-test, $p<0.05$), but several only responded to white
316 noise (49 of 185 sites). The example in figure 4 shows a penetration in which all of the sites
317 responded to tonal stimuli (t-test on tone trials, $p<0.05$) but showed no clear preference for
318 frequency among these responses. Responses to white noise were larger than those of tones
319 (red trace compared with blue trace in PSTH inset), particularly at the two deepest sites, as
320 would be expected of neurons with broad tuning characteristics.

321 To be sure that sites showing only transient responses to tones were not mistakenly
322 labeled as untuned due to the large window used for assessing tuning (for example, note the
323 relatively weak sustained component of the responses shown in the PSTH insets of figure 4),
324 we repeated the Gaussian fitting procedure using a shorter spike-counting window (10-50 ms
325 following stimulus onset). The majority of sites that showed tuning in one window also showed
326 tuning in the other (405 of 520 sites showed tuning in both windows, 66 showed tuning only in

the shorter window, 49 showed tuning only in the longer window). At tuned sites, estimates of BF were highly similar (t-test, $p>0.05$; supplemental figure 1).

Top-down maps of the categories of penetrations for each monkey are shown in figure 5. Each square in the maps corresponds to a single recording penetration location. The rows in the map for monkey A correspond to the panels shown in figure 1, with the columns within each row matching the electrode trajectories. In each monkey we collected data from a region showing auditory responses, surrounded to some extent by recordings from non-responsive cells. Responsive locations agreed well with estimates of the posterior, caudal and medial boundaries determined using MRI +/- 1mm (thick black lines). For grid holes with multiple penetrations, only the most tonotopic, tuned, or responsive penetration is depicted here. Supplementary figures 2-7 show the raw data used to generate these maps.

Tonotopic, tuned, and untuned penetrations were distributed in a characteristic pattern in the IC. Tonotopic penetrations (green) were only identified in 4 of 6 monkeys (A, W, M and C), When found, tonotopy tended to be located at or near the caudal extent of the region showing auditory responses or the MRI-identified posterior border. Adjacent to or surrounding the tonotopic penetrations were tuned penetrations (red), which account for the majority of penetrations in all monkeys. Untuned penetrations (blue) were most prominent in monkey A at the rostral extent of our sampling, but were occasionally observed in the other monkeys and at other (peripheral) locations.

Tuning of Non-tonotopic Penetrations

In recording penetrations that did not show a progression from low to high frequencies as the electrode advanced, but did show tuning, most sites responded best to the lowest frequencies

we tested. Figure 6A shows the distribution of BF values determined by Gaussian fits to the frequency response function data (see methods and examples in figures 2-3) in each monkey. The data set for this analysis involved one penetration per location, to avoid biasing estimates due to repeated sampling of some locations . With the exception of monkey W, all animals showed a powerful bias toward low frequency BFs throughout recordings. In a subset of recordings from monkey W we probed for BFs below the range tested in the other animals, to determine if this monkey had a low frequency bias but for lower frequencies than the other monkeys, but this did not appear to be the case. The vast majority of data from monkeys A,E,M,C and X, showed the most vigorous response to frequencies under 1.6kHz, several octaves below the upper limit of the monkey's hearing range (Stebbins et al. 1966). This is a surprising result, as no previous experiments have shown such a powerful bias toward low frequency tuning in the monkey, though many other species have auditory neurons that do show a bias toward a specific frequency range (eg. bat (Kossl and Vater 1985), mole (Muller et al. 1992), owl (Köppl et al. 1993)).

This bias in favor of low frequencies was also observed when the "point image" of activity in response to sound frequency was considered. The point image can be defined as the population response as a function of sound frequency, here expressed as the percentage of neurons responding to each tested frequency. Figure 6B shows the proportion of sites that responded to each frequency for each monkey. The curves show a strong bias toward low frequency responses, except for those describing the data from monkey W. Importantly, virtually all of the frequencies we tested elicited a response in some sites in each monkey, which reassures that the bias for low frequencies does not reflect complete loss of hearing at high frequencies. The macaque auditory midbrain thus seems to show an enhanced response to low frequencies. Responses to high frequencies are still present, though they rarely exceed the

magnitude of their low frequency counterparts. In this manner high frequency auditory information is not lost despite an amplification of low frequency information.

Temporal Response Profile

The temporal profile of a response provides an alternative to tuning characteristics in defining a functional map. The responses we recorded reliably showed an excitatory transient onset element, which was often followed by a sustained response (of varying magnitude) that continued throughout the presentation of the sound. We defined an index to measure the ratio of sustained to transient components (RPI, see methods), in order to see if response patterns were organized topographically. Figure 7 shows the maps of this index across recording penetrations from each monkey. The measures used for calculating RPI are indicated in the inset with two example PSTHs. Monkeys A and W show a large range in RPI, with the most sustained responses (lower RPI values) in locations near tonotopic penetrations. Monkeys M and C show less variability in response profile, but still show a strong coupling between sustained and tonotopic penetrations. The data from monkeys E and X, in which we did not find tonotopy, had surprisingly low RPI values, with responses as sustained as those in tonotopic penetrations in other monkeys.

We also observed variation in response profile within tonotopic penetrations. The example shown in figure 3 indicates various levels of sustained responses from depth to depth. The maps in figure 7 are collapsed across recording depths, and so topographic effects within electrode penetrations cannot be seen. Figure 8A shows the average RPI across the depth of recordings, relative to the depth of the first auditory response (ie. entry into the nucleus). Non-tonotopic penetrations showed little effect of depth. Conversely, tonotopic penetrations tended

to exhibit more transient responses at shallow depths (similar to those of non-tonotopic penetrations), while sites recorded deeper showed more sustained responses.

Figure 8B shows histograms of RPI from sites in tonotopic and non-tonotopic penetrations. While sites within tonotopic penetrations (red solid line) showed RPI values that were skewed toward lower numbers (ie. more sustained responses) than those within non-tonotopic penetrations (blue solid line), the distributions largely overlapped. Restricting the estimate of RPI from tonotopic penetrations to those deeper than the first site (red dashed line) shifted the distribution slightly to the left, and restricting the analysis of non-tonotopic sites to those monkeys that showed tonotopy (blue dashed line) shifted the distribution slightly to the right, but considerable overlap remained.

Latency of response also showed some topographic organization. More central penetrations contained sites that responded faster than more peripheral penetrations (figure 9). As with RPI, we also found an effect of depth within tonotopic penetrations, with shallower sites showing slower responses than those recorded at deeper locations (figure 10A). Across all locations, a small difference between tonotopic and non-tonotopic penetrations was found (t-test, $p<0.01$; figure 10B). Excluding the shallowest tonotopic recording and the data from monkeys in which we did not observe tonotopy slightly increased the separation between distributions of latency, but there was considerable overlap (similar to the results found for RPI). Overall, the estimates of latency are similar to those noted previously (Ryan and Miller 1978; Zwiers et al. 2004), when taking into account that latency calculations included the time it took to for the sound to reach the ear (about 4ms, see methods).

Discussion

The results from this study provide the first extensive physiological map of the auditory midbrain in the monkey. We established a small volume of tissue in which tonotopic organization was readily identifiable, surrounded by a surprisingly large region that showed no such organization. In the latter, low frequency responses prevailed, indicating a strong bias toward low frequency tones. The two functionally identifiable regions we observed likely have anatomical correlates.

Subdivisions of the IC and the representation of sound frequency

Historically the IC has been divided into a central nucleus (ICC) and surrounding regions on the lateral (lateral nucleus, LN) and dorsal (DCIC) aspects (Morest 1964; Ramón y Cajal 1911; Rockel and Jones 1973a; b; c). Golgi impregnations have provided a thorough parcellation through the precise analysis of the spatial arrangement of both axons and dendrites, as was performed by Morest and Oliver in the cat (1984). Their study classified cells surrounding the ICC, not just those lateral and dorsal to the central nucleus, but also cells rostral, caudal and medial to the ICC.

The distinguishing feature of ICC is a series of fibrodendritic laminae, formed by the parallel dendritic fields of disc shaped neurons (Morest 1964). The layers seem to match tuning patterns, with the most dorsolateral layers corresponding to low frequency tuned neurons, with tuning to increasing frequencies found in successively ventromedial layers (see (Ehret and Schreiner 2005) for review). ICC primarily receives ascending input from the auditory brain stem (from the cochlear nucleus reviewed in (Cant 2005), and from the superior olivary complex and nuclei of the lateral lemniscus reviewed in (Schofield 2005)). Descending input from auditory cortex also projects to the ICC (Andersen et al. 1980). Projections from the ICC continue up

the auditory pathway where they synapse mainly on the ventral region of the medial geniculate body (MGB; (Calford and Aitkin 1983)).

In contrast, LN and DCIC have a more diffuse set of connections. These regions receive ascending auditory input via the ICC (Saldaña and Merchan 1992), but more weakly from brainstem sources (Aitkin et al. 1981; Coleman and Clerici 1987). DCIC and LN are more heavily innervated by auditory cortex, receiving more descending input than ICC (Andersen et al. 1980; Coleman and Clerici 1987; Diamond et al. 1969; Druga and Syka 1984a; b; Druga et al. 1997; Saldaña et al. 1996; Schofield 2009; Winer et al. 2002), In addition, LN receives nonauditory input from the somatosensory (Aitkin et al. 1978; Aitkin et al. 1981)) and visual (Coleman and Clerici 1987; Cooper and Young 1976) systems. The projections from the LN and DCIC also differ from those of the ICC. DCIC and LN do project to the MGB, like the ICC does, but they mainly synapse on cells in the medial and dorsal regions (Calford and Aitkin 1983), along a purported modulatory pathway of the auditory system (Lee and Sherman 2010). These regions also send output to the SC ((Kudo and Niimi 1980).

Beyond the rostral borders of the ICC one finds the rostral pole (RP) and intercollicular tegmentum (Morest and Oliver 1984). RP is a small area that receives input from the auditory brainstem but differs from the ICC in that it sends its output primarily to the SC rather than the MGB (Harting and Van Lieshout 2000; Osen 1972). The intercollicular tegmentum is part of the mesencephalic reticular formation, and receives inputs from a variety of auditory, visual and somatosensory sources (Lopez et al. 1999; Robards 1979; RoBards et al. 1976).

The ICC thus forms an auditory “core” region that is an obligatory stop along the ascending auditory pathway – i.e. little or no input reaches the ventral auditory thalamus without first passing through the ICC. The surrounding structures form a “shell” region (LN, DCIC, RP,

intercollicular tegmentum) that receives auditory and non-auditory input from a variety of sources and projects more diffusely.

Because of the interconnectedness of the regions of the IC as a whole, the feedback they receive from auditory cortical regions, and the reciprocity of their connections with earlier brainstem auditory structures (Coleman and Clerici 1987; Gonzalez-Hernandez et al. 1996; Hutson et al. 1991; Saldaña and Merchan 1992), it is difficult to identify the circuit underlying any particular type of response. Nevertheless, certain physiological differences have been observed in these different regions. Aitkin and colleagues (1975) tested tuning and binaural response properties in cat ICC, DCIC, and LN. They found that neurons in DCIC and LN showed broad tuning, or no evidence of tuning at all, and that neurons in DCIC were generally only driven by the stimulation of the contralateral ear, while LN and ICC were binaurally influenced. DCIC and LN also seem to be better driven by complex sounds, such as vocalizations, while ICC neurons show greater firing in response to presentations of pure tones (Aitkin et al. 1994).

The tonotopic penetrations in our map likely passed through the ICC. ICC has exhibited clear tonotopic organization across species (eg. rats (Clopton and Winfield 1973; Kelly et al. 1991); cats (Aitkin et al. 1975; Merzenich and Reid 1974; Rose et al. 1963); guinea pigs (Malmierca et al. 1995); mice (Stiebler and Ehret 1985);; ferrets (Moore et al. 1983); owls (Knudsen and Konishi 1978); bats (Casseday and Covey 1992; Miller et al. 2005; Poon et al. 1990; Zook et al. 1985)), and shows more sustained and short latency responses (Aitkin et al. 1994; Ryan and Miller 1978; Syka et al. 2000; Willott and Urban 1978). Figure 11A shows an electrolytic lesion placed in the middle of a tonotopic penetration in monkey W, in a section stained with cytochrome oxidase. This stain marks metabolic activity, which is markedly higher in the ICC than in the surrounding area (Dezso et al. 1993). The location of the penetration in which the lesion was placed is indicated with an asterisk on the map in figure 5.

While the evidence that the tonotopic penetrations probably passed through the ICC is strong, the converse, that the non-tonotopic penetrations did not, is less clear. In monkeys E and X we did not identify tonotopic gradients in any recording penetrations. This is not surprising in monkey E, as our entire sample was likely medial to the ICC, but tonotopic organization was expected in monkey X where the central region was well sampled. A lesion was made at a central recording location and identified near RP on a section stained with Nissl techiniques (figure 11 B,C). Recordings were taken caudal to the location of the lesion, in a region that corresponds to ICC, but no tonotopic penetrations were identified, even though response characteristics typical of tonotopic penetrations in other monkeys, such as a strong sustained response or short response latency, were observed at several sites in monkey X.

It is therefore possible that the strength of tonotopic organization varies across individual animals and that in monkey X it was not identifiable, or that some aspect of our recording methods precluded detection of tonotopy. Improvements in our recording equipment over the course of this study may have facilitated identification of tonotopy, and responses in general. After testing monkeys X, C, M, and E, but before testing monkeys A and W, the neural recording system was upgraded and changes in software that allowed online analysis of the data were incorporated. This helped us target our recordings to the region of the IC more successfully, and improved our selection of multi-unit activity. Indeed, monkeys A and W showed the clearest signal to noise ratios. Interpretation and resolution of anatomical MRIs also improved throughout the course of the study, allowing better targeting of the IC.

Most likely, some but not all of the penetrations classified as non-tonotopic passed through the ICC as well. In particular, penetrations adjacent to tonotopic locations in our map likely passed through the ICC, but only through a small part, or passed through the ICC non-perpendicularly to the tonotopic gradient. It is also possible that a portion of the ICC is not

tonotopic at all but consistently favors low frequency sounds, and that this low frequency bias is a feature shared in common with the surrounding shell.

It is also possible that some locations that were actually tonotopic or tuned were mischaracterized due to the relatively coarse sampling of tissue relative to the size of the IC and the use of a set of stimuli that only represent part of the macaque frequency range. Although we only sampled a subset of the primate hearing range, this is unlikely to account for the low frequency bias we observed. Very few sites responded well to frequencies in the 2-12 kHz range; instead most sites responded best to lower frequencies. Since we did not test with higher frequencies, we cannot rule out that they showed bimodal frequency response functions with both low and very high frequency peaks, but there is little evidence of this kind of tuning pattern in other species. More likely, there may have been non-responsive sites at the end of tonotopic penetrations that were tuned to frequencies we did not test. The main confound produced by such an effect would be that the IC may be larger and the tonotopic stretches longer than we have been able to demonstrate.

Overall, identifying the location of any non-ICC penetrations is more challenging. Though measurements of the tonotopic region recorded fit well with estimates of the size of ICC (Paxinos et al. 2000), the auditory-responsive region surrounding tonotopic responses is much larger than anticipated, even when excluding potential ICC penetrations that were adjacent those in which tonotopy was identified. It is possible that some auditory responsive sites reflected signals from axons rather than cell bodies and this could have expanded the apparent size of the IC. Alternatively, these data are best described as coming from a number of nearby, anatomically distinct areas, including not only DCIC/LN but also regions such as the intercollicular tegmentum and the nucleus of the brachium. The homogeneity of response characteristics (latency, temporal profile, tuning properties), provides reason to group this data together, though it likely represents responses of both collicular and peri-collicular regions.

Temporal profile

The temporal patterns of the response also relate to those found previously. We found shorter-latency and more sustained responses in tonotopic penetrations (figures 8B and 10B). Along tonotopic penetrations, the most dorsal recordings showed uncharacteristically slow and transient responses (figures 8A and 10A), consistent with the idea that electrodes passed through DCIC en route to ICC. Results regarding the temporal profile should be compared with the literature with caution, as the choice of MUA as a metric precludes the identification of individual sustained and transient type cells. Rather, the measurement of sustained and transient components in the response relates to the proportion of sustained and transient type units comprising the MUA. Our data on responses in the awake animal also likely differ from those in anesthetized animals. Anesthesia has been shown to affect the temporal profile of responses in the IC (Astl et al. 1996; Kuwada et al. 1989).

Low frequency bias

The most surprising aspect of our findings was the prevalence of low frequency tuning. Throughout the more transient, slower, non-tonopic region we sampled, we found a strong bias toward low frequency tuning (figure 6). Fitzpatrick (1975) also found no evidence of high frequency tuned neurons (>2kHz) in the shell surrounding the ICC of the squirrel monkey.

Typically, the magnification of a particular range of stimulus-space corresponds with some enhanced perceptual capacity. For example, amplification of a specific frequency range, linked with sounds of ethological relevance has been seen in the auditory system of other species (eg. owl:(Köppl et al. 1993); bat: (Kossl and Vater 1985); mole: (Muller et al. 1992)).

This finding is surprising in rhesus monkeys because no perceptual correlate in this frequency range has yet been established. The rhesus monkey audiogram is approximately flat from 500 Hz to 16 kHz: the monkey is at its most sensitive, and uniformly so, throughout this range (for review see (Coleman 2009)). That a perceptual or ethological correlate may eventually be found seems possible: preliminary efforts in our lab to train monkeys to perform sound frequency discrimination tasks have been more successful at lower frequencies, ~800 Hz, than at higher frequencies, ~3 kHz (Ross and Groh 2009).

Implications for prostheses and other work

Several aspects of our study have important implications for the design and placement of prosthetic devices in the inferior colliculus. Chiefly, the limited extent of tonotopy, the variability in its presence or perhaps location in individual animals, and the dominance of low frequencies pose a logistical challenge. To be successful, a prosthetic device needs to access sites that encode a range of different frequencies. It may also be advantageous to target the main channels of the ascending auditory signal. If the human IC is similar to that of the monkey, then a large number of electrodes may need to be placed in a range of locations in order to increase the odds that some are positioned in the comparatively small volume of the IC containing neurons devoted to ascending high frequency information. Indeed, the earliest attempts at auditory midbrain implants have produced predominantly low frequency percepts at most electrode sites (Lim et al. 2008), suggesting that the challenge of finding high frequency sites may well be true in humans as well as monkeys.

Generally, our results provide a guide or context that may be of some utility for studies in which detailed mapping is not possible. Placement of prosthetic stimulating electrodes in humans is done precisely because the patient is deaf without it – thus mapping the auditory

response properties prior to placement is not possible. Other types of work involve a trade-off between optimizing for anatomical certainty at the expense of physiological normality and vice versa. For example, the most detailed mapping studies are generally done in anesthetized animals, over the span of at most a few days, and often involve removal of the tissue overlying the inferior colliculus so that the placement of the electrodes can be guided by visual inspection. Histological reconstruction is done immediately following such experiments. Such methods provide the best information about the location of recording sites, but the information about the response properties is colored by uncertainty about whether the response properties are altered by the presence of anesthetic drugs or the removal of a portion of the brain. At the other end of the spectrum are studies in which no mapping is conducted and the response properties are studied largely divorced from information about where precisely they may occur. In awake monkeys, recordings take place over months or years, making it very difficult to reconstruct the location of specific sites even if histology is conducted at the conclusion of the studies. Our study attempted to strike a middle ground between these approaches.

Our study also represents a relatively coarse sampling of the midbrain. This was necessary to accommodate the large region of auditory-responsive neurons. Our map thus describes the large scale organization of the midbrain, but cannot precisely identify boundaries, or the three-dimensional shape of functionally defined regions. Such a coarse approach was required to collect a body of data that sampled the entire IC, including measurements of activity from outside the IC so that functional borders could be determined. Finer spatial sampling, and additional stimulus characteristics would have added to the resolution of the map, but are unrealistic in such large scale systematic mapping. The objective methods we used for categorizing tonotopic penetrations, and temporal profile of response provide metrics that can be compared across electrophysiological studies. Our results can thus be used to guide future

611 work focused on a limited region of the IC, and provide a context for interpreting organization at
612 a smaller scale.

613

Acknowledgements

We thank Nate Greene, Vanessa Kennedy, Uri Werner-Reiss, and Nick Del Grosso for collecting some of the data for these experiments; Abigail Underhill, Tom Heil, and Jessi Cruger for technical support; and Nell Cant, David Larue, and Jeff Winer for performing the histology. We also thank Nell Cant, David Larue, Jeff Winer, David Fitzpatrick, Michael Platt, and Steve Mitroff for insightful comments.

Grants

This research was supported by the National Institutes of Health grants EY016478, (to JMG) and DC010294 (to DAB).

625

626 References

627

628 **Aitkin L, Tran L, and Syka J**. The responses of neurons in subdivisions of the inferior
629 colliculus of cats to tonal, noise and vocal stimuli. *Exp Brain Res* 98: 53-64, 1994.
630 **Aitkin LM, Dickhaus H, Schult W, and Zimmermann M**. External nucleus of inferior
631 colliculus: auditory and spinal somatosensory afferents and their interactions. *J*
632 *Neurophysiol* 41: 837-847, 1978.
633 **Aitkin LM, Kenyon CE, and Philpott P**. The representation of the auditory and
634 somatosensory systems in the external nucleus of the cat inferior colliculus. *J Comp*
635 *Neurol* 196: 25-40, 1981.
636 **Aitkin LM, and Phillips SC**. Is the inferior colliculus and obligatory relay in the cat
637 auditory system? *Neuroscience Letters* 44: 259-264, 1984.
638 **Aitkin LM, Webster WR, Veale JL, and Crosby DC**. Inferior colliculus. I. Comparison
639 of response properties of neurons in central, pericentral, and external nuclei of adult cat.
640 *J Neurophysiol* 38: 1196-1207, 1975.
641 **Andersen RA, Snyder RL, and Merzenich MM**. The topographic organization of
642 corticocollicular projections from physiologically identified loci in the AI, AII, and anterior
643 auditory cortical fields of the cat. *J Comp Neurol* 191: 479-494, 1980.
644 **Astl J, Popelar J, Kvasnak E, and Syka J**. Comparison of response properties of
645 neurons in the inferior colliculus of guinea pigs under different anesthetics. *Audiology*
646 35: 335-345, 1996.
647 **Calford MB, and Aitkin LM**. Ascending projections to the medial geniculate body of the
648 cat: evidence for multiple, parallel auditory pathways through thalamus. *J Neurosci* 3:
649 2365-2380, 1983.
650 **Cant NB**. Projections from the Cochlear Nuclear Complex to the Inferior Colliculus. In:
651 *The Inferior Colliculus*, edited by Winer JA, and Schreiner CE. New York, NY: Springer,
652 2005, p. 115-131.
653 **Casseday JH, and Covey E**. Frequency tuning properties of neurons in the inferior
654 colliculus of an FM bat. *J Comp Neurol* 319: 34-50, 1992.
655 **Clopton BM, and Winfield JA**. Tonotopic organization in the inferior colliculus of the
656 rat. *Brain Res* 56: 355-358, 1973.
657 **Coleman JR, and Clerici WJ**. Sources of projections to subdivisions of the inferior
658 colliculus in the rat. *J Comp Neurol* 262: 215-226, 1987.
659 **Coleman M**. What Do Primates Hear? A Meta-analysis of All Known Nonhuman
660 Primate Behavioral Audiograms. *International Journal of Primatology* 30: 55-91, 2009.
661 **Colletti V, Shannon R, Carner M, Sacchetto L, Turazzi S, Masotto B, and Colletti L**.
662 The first successful case of hearing produced by electrical stimulation of the human
663 midbrain. *Otol Neurotol* 28: 39-43, 2007.
664 **Colletti V, Shannon RV, Carner M, Veronese S, and Colletti L**. Progress in
665 restoration of hearing with the auditory brainstem implant. *Prog Brain Res* 175: 333-345,
666 2009.
667 **Cooper MH, and Young PA**. Cortical projections to the inferior colliculus of the cat. *Exp*
668 *Neurol* 51: 488-502, 1976.

669 **Dezso A, Schwarz DW, and Schwarz IE**. A survey of the auditory midbrain, thalamus
670 and forebrain in the chicken (Gallus domesticus) with cytochrome oxidase
671 histochemistry. *J Otolaryngol* 22: 391-396, 1993.
672 **Diamond IT, Jones EG, and Powell TP**. The projection of the auditory cortex upon the
673 diencephalon and brain stem in the cat. *Brain Res* 15: 305-340, 1969.
674 **Druga R, and Syka J**. Ascending and descending projections to the inferior colliculus in
675 the rat. *Physiol Bohemoslov* 33: 31-42, 1984a.
676 **Druga R, and Syka J**. Neocortical projections to the inferior colliculus in the rat. (An
677 experimental study using anterograde degeneration techniques). *Physiol Bohemoslov*
678 33: 251-253, 1984b.
679 **Druga R, Syka J, and Rajkowska G**. Projections of auditory cortex onto the inferior
680 colliculus in the rat. *Physiol Res* 46: 215-222, 1997.
681 **Ehret G, and Schreiner CE**. Spectral and Intensity Coding in the Auditory Midbrain. In:
682 *The Inferior Colliculus*, edited by Winer JA, and Schreiner CE. New York, NY: Springer,
683 2005, p. 312-345.
684 **FitzPatrick KA**. Cellular architecture and topographic organization of the inferior
685 colliculus of the squirrel monkey. *J Comp Neurol* 164: 185-207, 1975.
686 **Gonzalez-Hernandez T, Mantolan-Sarmiento B, Gonzalez-Gonzalez B, and Perez-**
687 **Gonzalez H**. Sources of GABAergic input to the inferior colliculus of the rat. *J Comp*
688 *Neurol* 372: 309-326, 1996.
689 **Groh JM, Kelly KA, and Underhill AM**. A monotonic code for sound azimuth in primate
690 inferior colliculus. *J Cogn Neurosci* 15: 1217-1231, 2003.
691 **Groh JM, Trause AS, Underhill AM, Clark KR, and Inati S**. Eye position influences
692 auditory responses in primate inferior colliculus. *Neuron* 29: 509-518, 2001.
693 **Harting JK, and Van Lieshout DP**. Projections from the rostral pole of the inferior
694 colliculus to the cat superior colliculus. *Brain Res* 881: 244-247, 2000.
695 **Hutson KA, Glendenning KK, and Masterton RB**. Acoustic chiasm. IV: Eight midbrain
696 decussations of the auditory system in the cat. *J Comp Neurol* 312: 105-131, 1991.
697 **Jay MF, and Sparks DL**. Auditory receptive fields in primate superior colliculus shift
698 with changes in eye position. *Nature* 309: 345-347, 1984.
699 **Jay, MF and Sparks DL.** Sensorimotor integration in the primate superior colliculus. I.
700 Motor convergence. *J Neurophysiol* 57:22-34, 1987.
701 **Jay, MF and Sparks DL.** Sensorimotor integration in the primate superior colliculus. II.
702 Coordinates of auditory signals. *J Neurophysiol* 57:35-55, 1987.
703 **Judge SJ, Richmond BJ, and Chu FC**. Implantation of magnetic search coils for
704 measurement of eye position: an improved method. *Vision Res* 20: 535-538, 1980.
705 **Kalwani RM, Bloy L, Elliott MA, and Gold JI**. A method for localizing microelectrode
706 trajectories in the macaque brain using MRI. *J Neurosci Methods* 176: 104-111, 2009.
707 **Kelly JB, Glenn SL, and Beaver CJ**. Sound frequency and binaural response
708 properties of single neurons in rat inferior colliculus. *Hear Res* 56: 273-280, 1991.
709 **Knudsen EI, and Konishi M**. Space and frequency are represented separately in
710 auditory midbrain of the owl. *J Neurophysiol* 41: 870-884, 1978.
711 **Köppl C, Gleich O, and Manley G**. An auditory fovea in the barn owl cochlea. *Journal*
712 *of Comparative Physiology A: Neuroethology, Sensory, Neural, and Behavioral*
713 *Physiology* 171: 695-704, 1993.

Kossl M, and Vater M. The cochlear frequency map of the mustache bat, Pteronotus parnellii. *J Comp Physiol A* 157: 687-697, 1985.
Kudo M, and Niimi K. Ascending projections of the inferior colliculus in the cat: an autoradiographic study. *J Comp Neurol* 191: 545-556, 1980.
Kuwada S, Batra R, and Stanford TR. Monaural and binaural response properties of neurons in the inferior colliculus of the rabbit: effects of sodium pentobarbital. *J Neurophysiol* 61: 269-282, 1989.
Lee CC, and Sherman SM. Drivers and modulators in the central auditory pathways. *Front Neurosci* 4: 79, 2010.
Lim HH, and Anderson DJ. Auditory cortical responses to electrical stimulation of the inferior colliculus: implications for an auditory midbrain implant. *J Neurophysiol* 96: 975-988, 2006.
Lim HH, and Anderson DJ. Spatially distinct functional output regions within the central nucleus of the inferior colliculus: implications for an auditory midbrain implant. *J Neurosci* 27: 8733-8743, 2007.
Lim HH, Lenarz M, and Lenarz T. Auditory midbrain implant: a review. *Trends Amplif* 13: 149-180, 2009.
Lim HH, Lenarz T, Anderson DJ, and Lenarz M. The auditory midbrain implant: effects of electrode location. *Hear Res* 242: 74-85, 2008.
Lopez DE, Saldaña E, Nodal FR, Merchan MA, and Warr WB. Projections of cochlear root neurons, sentinels of the rat auditory pathway. *J Comp Neurol* 415: 160-174, 1999.
Malmierca MS, Rees A, Le Beau FE, and Bjaalie JG. Laminar organization of frequency-defined local axons within and between the inferior colliculi of the guinea pig. *J Comp Neurol* 357: 124-144, 1995.
Merzenich MM, and Reid MD. Representation of the cochlea within the inferior colliculus of the cat. *Brain Res* 77: 397-415, 1974.
Miller KE, Casseday JH, and Covey E. Relation between intrinsic connections and isofrequency contours in the inferior colliculus of the big brown bat, Eptesicus fuscus. *Neuroscience* 136: 895-905, 2005.
Moore BCJ. *An introduction to the psychology of hearing*. Bingley: Emerald, 2008, p. 1 vol. (XIIII-413 p.).
Moore DR, Semple MN, and Addison PD. Some acoustic properties of neurones in the ferret inferior colliculus. *Brain Res* 269: 69-82, 1983.
Morest DK. Laminar Structure of Inferior Colliculus of Cat. *Anat Rec* 148: 314-&, 1964.
Morest DK, and Oliver DL. The neuronal architecture of the inferior colliculus in the cat: defining the functional anatomy of the auditory midbrain. *J Comp Neurol* 222: 209-236, 1984.
Muller M, Laube B, Burda H, and Bruns V. Structure and function of the cochlea in the African mole rat (Cryptomys hottentotus): evidence for a low frequency acoustic fovea. *J Comp Physiol A* 171: 469-476, 1992.
Osen KK. Projection of the cochlear nuclei on the inferior colliculus in the cat. *J Comp Neurol* 144: 355-372, 1972.
Paxinos G, Huang XF, and Toga AW. *The rhesus monkey brain in stereotaxic coordinates*. San Diego, CA: Academic Press, 2000, p. 163 p.
Pfingst BE, Hienz R, and Miller J. Reaction-time procedure for measurement of hearing. II. Threshold functions. *J Acoust Soc Am* 57: 431-436, 1975.

Pfingst BE, Laycock J, Flammino F, Lonsbury-Martin B, and Martin G. Pure tone thresholds for the rhesus monkey. *Hear Res* 1: 43-47, 1978.
Poon PW, Sun X, Kamada T, and Jen PH. Frequency and space representation in the inferior colliculus of the FM bat, Eptesicus fuscus. *Exp Brain Res* 79: 83-91, 1990.
Populin LC, Tollin DJ, and Yin TC. Effect of eye position on saccades and neuronal responses to acoustic stimuli in the superior colliculus of the behaving cat. *J Neurophysiol* 92: 2151-2167, 2004.
Porter KK, Metzger RR, and Groh JM. Representation of eye position in primate inferior colliculus. *J Neurophysiol* 95: 1826-1842, 2006.
Porter KK, Metzger RR, and Groh JM. Visual- and saccade-related signals in the primate inferior colliculus. *Proc Natl Acad Sci U S A* 104: 17855-17860, 2007.
Ramón y Cajal S. *Histologie du système nerveux de l'homme et des vertébrés, Vol. 1*. Paris: A. Maloine, 1911, p. 997 p.
Robards MJ. Somatic neurons in the brainstem and neocortex projecting to the external nucleus of the inferior colliculus: an anatomical study in the opossum. *J Comp Neurol* 184: 547-565, 1979.
RoBards MJ, Watkins DW, 3rd, and Masterton RB. An anatomical study of some somesthetic afferents to the intercollicular terminal zone of the midbrain of the opossum. *J Comp Neurol* 170: 499-524, 1976.
Robinson DA. A Method of Measuring Eye Movement Using a Scleral Search Coil in a Magnetic Field. *IEEE Trans Biomed Eng* 10: 137-145, 1963.
Rockel AJ, and Jones EG. The neuronal organization of the inferior colliculus of the adult cat. I. The central nucleus. *J Comp Neurol* 147: 11-60, 1973a.
Rockel AJ, and Jones EG. The neuronal organization of the inferior colliculus of the adult cat. II. The pericentral nucleus. *J Comp Neurol* 149: 301-334, 1973b.
Rockel AJ, and Jones EG. Observations on the fine structure of the central nucleus of the inferior colliculus of the cat. *J Comp Neurol* 147: 61-92, 1973c.
Rose JE, Greenwood DD, Goldberg JM, and Hind JE. Some discharge characteristics of single neurons in the inferior colliculus of the cat. I. Tonotopical organization, relation of spike-counts to tone intensity, and firing patterns of single elements. *J Neurophysiol* 26: 294-320, 1963.
Ross DA, and Groh JM. Performance of monkeys on a frequency discrimination task involving pitch direction (higher vs. lower) judgments. In: *Society for Neuroscience Annual Meeting*. Chicago, IL: 2009.
Ryan A, and Miller J. Single unit responses in the inferior colliculus of the awake and performing rhesus monkey. *Exp Brain Res* 32: 389-407, 1978.
Saldaña E, Feliciano M, and Mugnaini E. Distribution of descending projections from primary auditory neocortex to inferior colliculus mimics the topography of intracollicular projections. *J Comp Neurol* 371: 15-40, 1996.
Saldaña E, and Merchan MA. Intrinsic and commissural connections of the rat inferior colliculus. *J Comp Neurol* 319: 417-437, 1992.
Schofield BR. Projections to the inferior colliculus from layer VI cells of auditory cortex. *Neuroscience* 159: 246-258, 2009.
Schofield BR. Superior Olivary Complex and Lateral Lemniscal Connections of the Auditory Midbrain. In: *The Inferior Colliculus*, edited by Winer JA, and Schreiner CE. New York, NY: Springer, 2005, p. 132-154.

Stebbins WC, Green S, and Miller FL. Auditory sensitivity of the monkey. *Science* 153: 1646-1647, 1966.
Stiebler I, and Ehret G. Inferior colliculus of the house mouse. I. A quantitative study of tonotopic organization, frequency representation, and tone-threshold distribution. *J Comp Neurol* 238: 65-76, 1985.
Syka J, Popelar J, Kvasnak E, and Astl J. Response properties of neurons in the central nucleus and external and dorsal cortices of the inferior colliculus in guinea pig. *Exp Brain Res* 133: 254-266, 2000.
Wessberg J, Stambaugh CR, Kralik JD, Beck PD, Laubach M, Chapin JK, Kim J, Biggs SJ, Srinivasan MA, and Nicolelis MAL. Real-time prediction of hand trajectory by ensembles of cortical neurons in primates. *Nature* 408: 361-365, 2000.
Willott JF, and Urban GP. Response properties of neurons in nuclei of the mouse inferior colliculus. *Journal of Comparative Physiology A: Neuroethology, Sensory, Neural, and Behavioral Physiology* 127: 175-184, 1978.
Winer JA, Chernock ML, Larue DT, and Cheung SW. Descending projections to the inferior colliculus from the posterior thalamus and the auditory cortex in rat, cat, and monkey. *Hear Res* 168: 181-195, 2002.
Zook JM, Winer JA, Pollak GD, Bodenhamer RD. Topology of the central nucleus of the mustache bat's inferior colliculus: correlation of single unit properties and neuronal architecture. *J Comp Neurol*, 231: 530-46, 1985.
Zwiers MP, Versnel H, and Van Opstal AJ. Involvement of monkey inferior colliculus in spatial hearing. *J Neurosci* 24: 4145-4156, 2004.

Figure Captions

Table 1. Quantity and Categorization of Recordings. The total number of recorded and responsive locations is shown, along with the number assigned to each penetration category as described in methods and shown in Figure 5. In cases where penetration locations were sampled more than once, both the raw totals and the number of unique penetration locations are shown. If any tonotopic penetrations were observed at a given grid location, the location was marked as tonotopic; if any tuned penetrations were observed, the location was marked as tuned.

Figure 1 The locations mapped in monkey A illustrated on MR images. A series of coronal MR images spanning the 10mm range that was sampled physiologically. Voxels were 0.5mm cubes. Images were rotated into the plane of recording by placing electrodes in the recording grid, visible around 0mm and 7mm, Each panel corresponds to a single mediolateral row of grid locations at a given position in the anterior/posterior dimension (interleaved coronal slices are not displayed). Red lines indicate the approach of each of the recording locations in the medial/lateral dimension. Green lines indicate the targeted area; recordings shallower and deeper than these borders were discarded. The locations of the IC and SC are indicated on two of the panels.

Figure 2 Responses from a tuned penetration. The average response over a 200ms period following baseline (normalized by subtracting the mean and dividing by the standard deviation of the activity during the baseline period) is plotted in blue as a function of sound frequency (ie. Isointensity frequency response curves). Error bars indicate standard error. The topmost panel shows the shallowest recording in this penetration, with each panel thereafter being 0.5mm deeper. A Gaussian curve (red line) was fit to data from tone trials. The location of the peak of this curve was labeled as BF, which remained low throughout this penetration. At the extreme

856 right of the figure, the average and standard error of responses to presentations of broadband
857 white noise are shown. Insets show the PSTH across stimuli for a period ranging from 50ms
858 before to 200ms after stimulus onset. Below the tuning data, results from a Monte Carlo
859 analysis to probe for tonotopy indicate that this penetration did not show an increase in BF with
860 deeper recordings: the slopes are not biased towards positive values.

861 Figure 3 Frequency responses from a tonotopic penetration. Plotted in the same format as
862 figure 2, the panels show an increase in BF with deeper recordings. All iterations of the Monte
863 Carlo analysis used to detect tonotopy showed positive slopes.

864 Figure 4 Frequency responses from an untuned penetration. Plotted in the same format as
865 figure 2, this penetration showed no clear tuning. Gaussian curves did not fit the data and so are
866 not plotted. Sites in this penetration responded to tones, but did not prefer a group of tone
867 frequencies over others. Here, the PSTH insets show firing rate changes over time separately
868 for noise (red trace) and tone (blue trace) trials. No inset is shown for the Monte Carlo analysis
869 used to detect tonotopy, as this analysis could not be run on untuned penetrations.

870 Figure 5 Maps of responsive, tuned, and tonotopic penetrations. Maps of penetration locations
871 (ie. the horizontal plane of the recording chamber) for each monkey. Each box in the maps
872 displays information for a single location in the recording chamber (boxes from monkey A
873 correspond to the red lines displayed in figure 1). Unfilled boxes indicate recordings in which
874 auditory responses were not found. Blue, red, and green boxes mark the locations of responsive
875 (but untuned), tuned (but non-tonotopic), and tonotopic recording penetrations. On occasions
876 where multiple recordings were made from the same location, the box is colored if any of the
877 penetrations met the criteria to be categorized as tonotopic, tuned, or responsive. Locations
878 marked with an ‘X’ on the maps for Monkeys W and X indicate the locations of electrolytic
879 lesions used for histological reconstruction.

Figure 6 Bias of tuning toward low frequencies throughout recordings. A shows the distribution of BF values determined by Gaussian fits to the isointensity frequency response data collected. Lines show the proportion of auditory sites that showed a BF in logarithmically spaced windows. B shows the proportion of neurons responding to each tested frequency. Both representations of the data indicate a heavy bias toward low frequency selectivity, though B establishes that virtually all of the tested frequencies elicited responses at some sites.

Figure 7 Maps of temporal profile of response in the horizontal plane. Maps follow the format in figure 5, here color indicates the average RPI from each penetration location. Lower values of RPI indicate more sustained responses. The inset shows the time periods used to calculate RPI with the data from two example recordings.

Figure 8 RPI distribution for tonotopic and non-tonotopic penetrations. Panel A shows the average RPI at each depth, relative to the first auditory recording within the penetration, for tonotopic (red) and non-tonotopic (blue) penetrations. Error bars indicate standard error. The distributions of RPI in tonotopic and non-tonotopic penetrations (B) overlapped, though tonotopic penetrations generally showed more sustained (ie. lower RPI) responses. The trend persisted when data from monkeys not showing tonotopy were excluded (blue broken line) or when the shallowest recordings were excluded (red broken line).

Figure 9 Maps of response latency in the horizontal plane. Maps follow the format in figure 5, here color indicates the average latency from each penetration location. Note that the calculation of latency included the time it took for sound to reach the ear (about 4 ms).

Figure 10 Latency distribution for tonotopic and non-tonotopic penetrations. Panel A shows the average latency at each depth, relative to the first auditory recording in the penetration, for tonotopic (red) and non-tonotopic (blue) penetrations. Error bars indicate standard error. The distributions of latency in tonotopic and non-tonotopic penetrations (B) overlapped, though

tonotopic penetrations generally showed more faster (ie. lower latency) responses. The trend persisted when data from monkeys not showing tonotopy were excluded (blue broken line) or when the shallowest recordings were excluded (red broken line).

Figure 11 Histological verification of recording locations. Panel A shows a 60 μm coronal section from monkey W stained with cytochrome oxidase. The location of an electrolytic lesion (noted on the map in figure 5) is indicated with a red asterisk. A track left behind by a recording electrode, approximately 1mm medial to the lesion and following the 30º angle established by the chamber, is indicated with a black asterisk. The ICC can be visualized as the region showing a dark stain, indicative of higher metabolic activity. A section from Monkey X is shown in B, in which two lesions were made along a penetration through the central region of recordings (the location is noted on the map in figure 5, and on the image with red asterisks). Sections from this monkey were 50 μm thick and stained with cresyl violet. The section containing the lesion is rostral to the one shown in A, and the SC is clearly identifiable on the dorsal part of the slide. Just deeper than the lesion the rostral pole can be found, indicating that this penetration was just anterior to the ICC. Panel C shows a magnified view of the square in B. The image shown in B and C has been published previously (Porter et al. 2006).

Supplementary Figure 1 Comparison of Temporal Windows for Defining Tuning.

BF was determined for each site (see methods) based on a 200ms window following stimulus onset, as well as based on a shorter window (10-60ms following stimulus onset). Sites in which tuning was defined for both windows showed highly similar estimates of BF, indicating that tuning was stable over time.

Supplementary Figure 2 Three Dimensional Representation for Tuning Curves Recorded in Monkey A.

Each panel shows a heatmap indicating the responses to each frequency (x axis) across depths (y axis) within penetrations from Monkey A. Lighter colors indicate a larger response, and the position of the panels indicates the location of recordings in the M/L and A/P dimensions (with a format matching figures 5,7, and 9). Blue shading indicates non-responsive or untested depths. In cases where a location was sampled more than once, the example with the clearest frequency tuning or tonotopy is shown, as described in the main text.

Supplementary Figure 3 Three Dimensional Representation for Tuning Curves Recorded in Monkey W.

Following the same conventions as supplementary figure 2.

Supplementary Figure 4 Three Dimensional Representation for Tuning Curves Recorded in Monkey E.

Following the same conventions as supplementary figure 2.

Supplementary Figure 5 Three Dimensional Representation for Tuning Curves Recorded in Monkey M.

Following the same conventions as supplementary figure 2.

Supplementary Figure 6 Three Dimensional Representation for Tuning Curves Recorded in Monkey C.

Following the same conventions as supplementary figure 2.

Supplementary Figure 7 Three Dimensional Representation for Tuning Curves Recorded in Monkey X.

Following the same conventions as supplementary figure 2.

949 Supplementary Figure 8 Three Dimensional Representation of Latency of Responses

950 The latency across each penetration is indicated, with shorter latency responses shown with
951 lighter colors and longer latencies with darker colors. The panels for each monkey are
952 organized in the same manner as in supplementary figures 2-7. Blue shading indicates non-
953 responsive or untested depths.

954 Supplementary Figure 9 Spectra of Sounds Used in Recordings

955 Spectra of pure tones, recorded from Audax Model TWO25V2 speakers used to collect data
956 from monkeys E,M,C and X. Recordings were collected with a microphone (Sennheiser
957 ME62/K6P) placed at the location normally occupied by the monkey's head, and sampled with a
958 PC sound card at 44.1kHz. The power scale (y axis) is in arbitrary units. Prior to these
959 measurements, the sounds were calibrated using a sound level meter to be at 50 dB SPL. The
960 noise floor of the recording booth was approximately 30 dB SPL.

961

962 **Table 1:**

		Monkey						
		A	W	E	M	C	X	Total
Recorded	Penetrations	59	50	51	74	42	74	350
	Sites	646	534	694	588	457	790	3709
Responsive	Penetrations	45	27	13	11	15	14	125
	Sites	247	134	61	49	71	77	639
Penetration Category	Untuned	16(10)	4(3)	1(1)	0	2(1)	0(0)	23(15)
	Tuned*	22(21)	13(11)	12(9)	6(6)	9(7)	14(14)	76(68)
	Tonotopic	7(5)	10(5)	0(0)	5(4)	4(3)	0(0)	26(17)

*Excluding tonotopic penetrations
**Numbers in parentheses indicate quantities of unique penetration locations

963

964

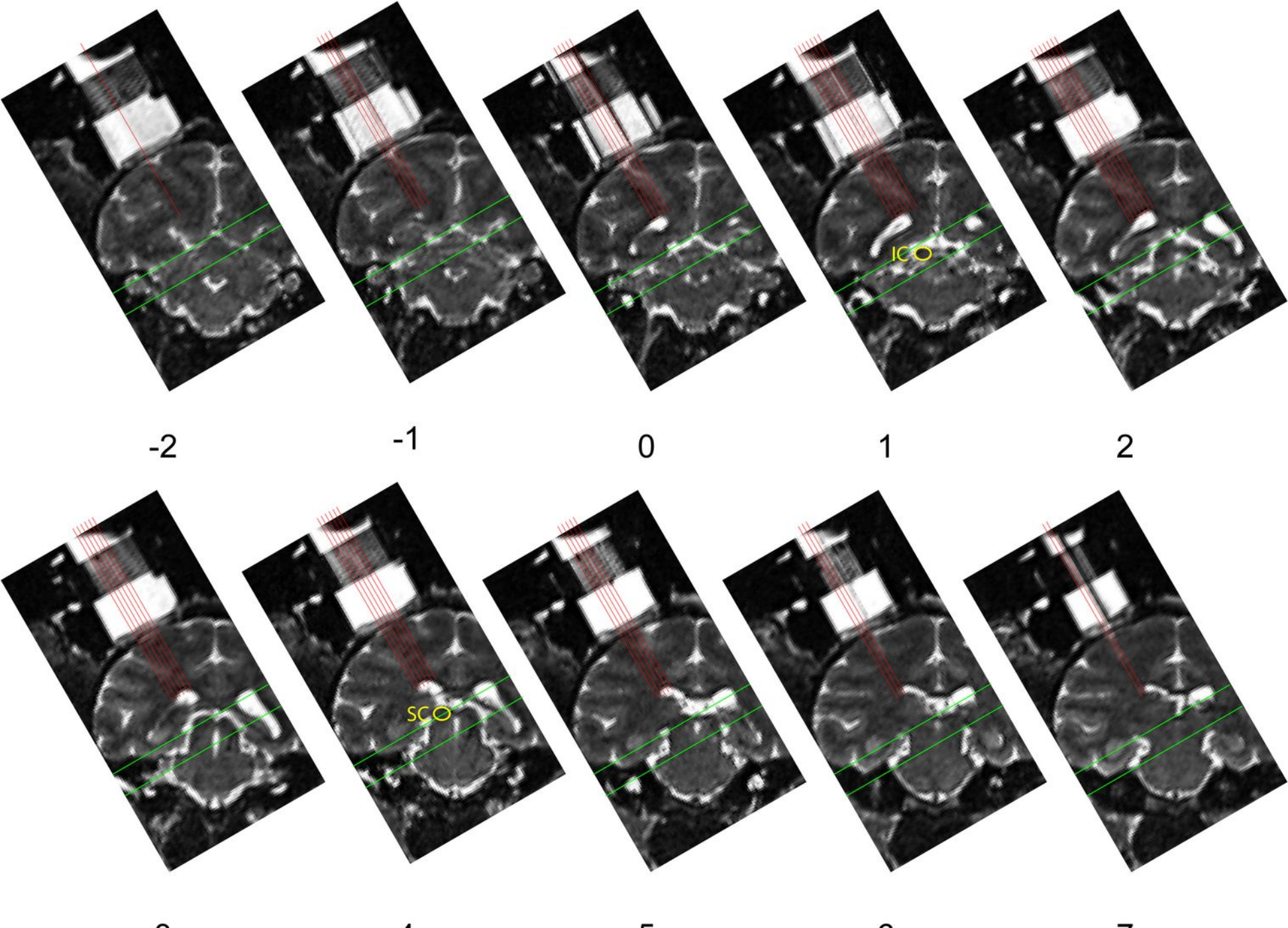
IC
SC
-2
-1
0
1
2
3
4
5
6
7
Distance To IC Caudal Boundary (mm)

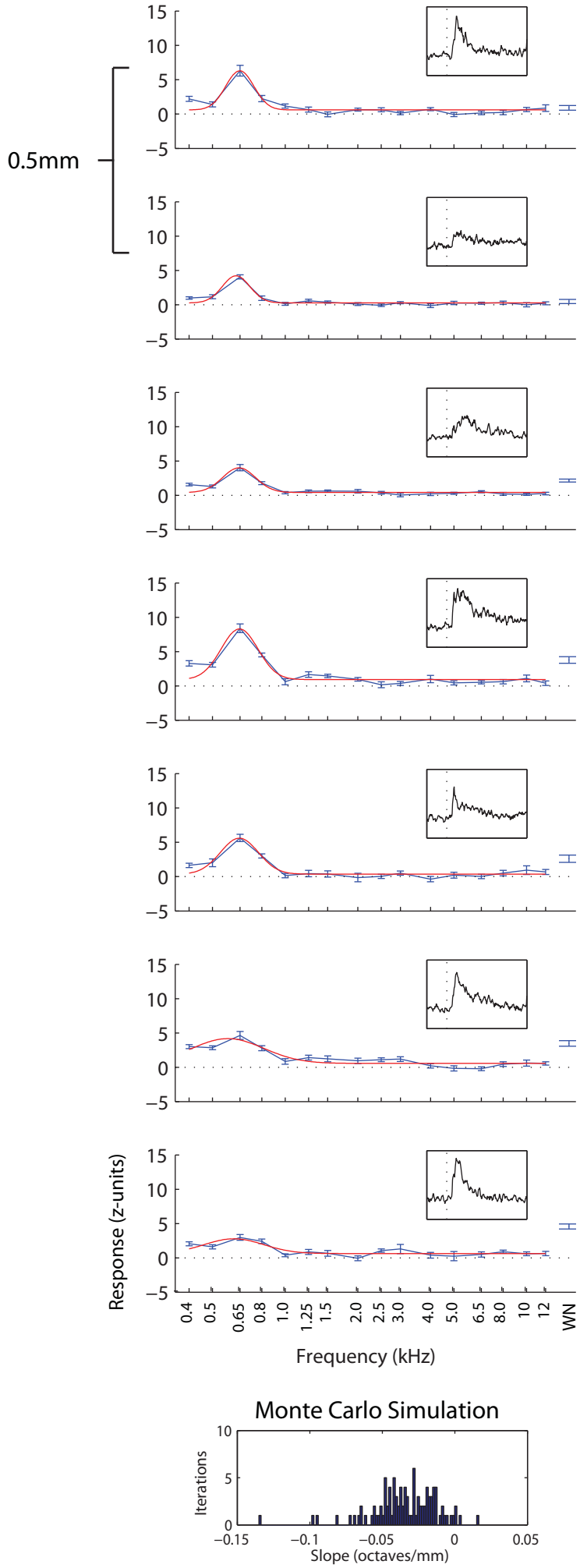
0.5mm
15
10
5
0
−5
Response (z-units)
0.4
0.5
0.65
0.8
1.0
1.25
1.5
2.0
2.5
3.0
4.0
5.0
6.5
8.0
10
12
WN
Frequency (kHz)
Monte Carlo Simulation
Iterations
10
5
0
−0.15
−0.1
−0.05
0
0.05
Slope (octaves/mm)

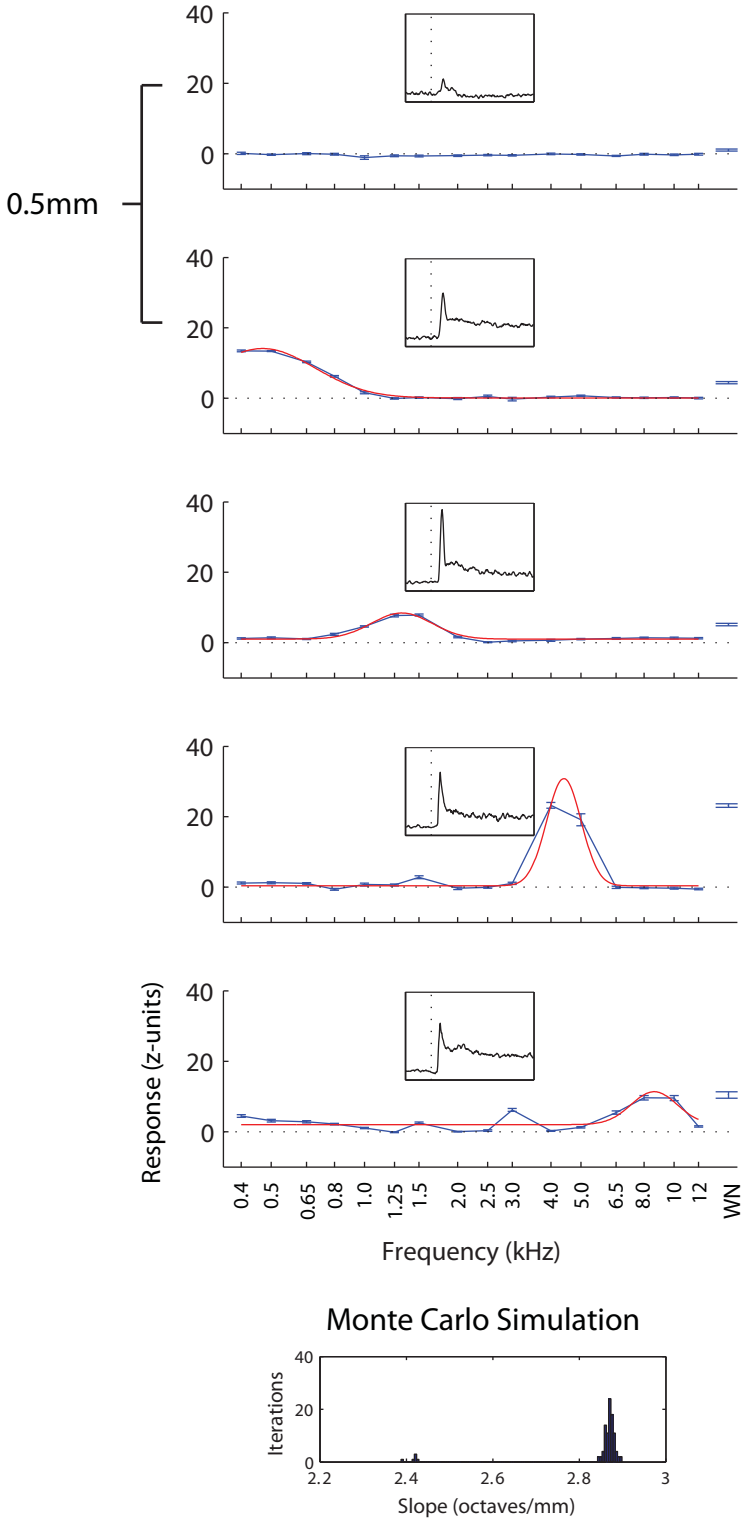
0.5mm
40
20
0
Response (z-units)
0.4
0.5
0.65
0.8
1.0
1.25
1.5
2.0
2.5
3.0
4.0
5.0
6.5
8.0
10
12
WN
Frequency (kHz)
Monte Carlo Simulation
Iterations
2.2
2.4
2.6
2.8
3
Slope (octaves/mm)

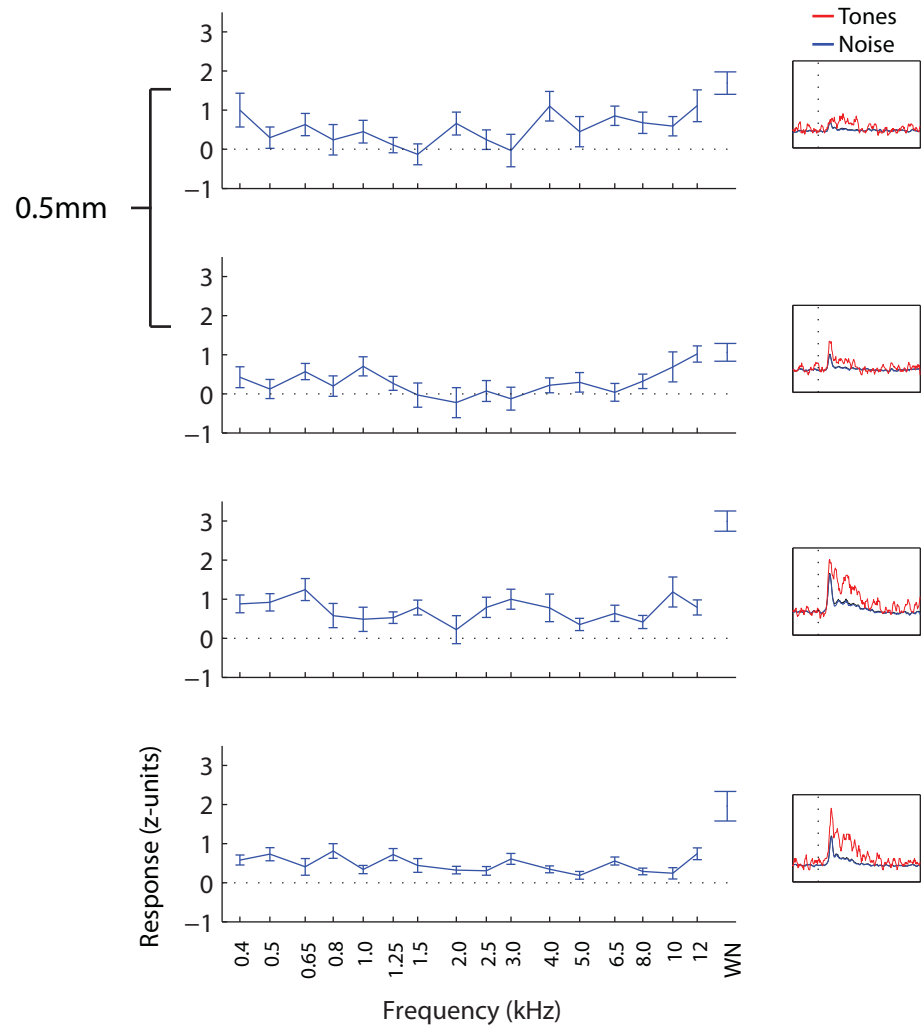
Tones
Noise
0.5mm
3
2
1
0
−1
Response (z-units)
0.4
0.5
0.65
0.8
1.0
1.25
1.5
2.0
2.5
3.0
4.0
5.0
6.5
8.0
10
12
WN
Frequency (kHz)

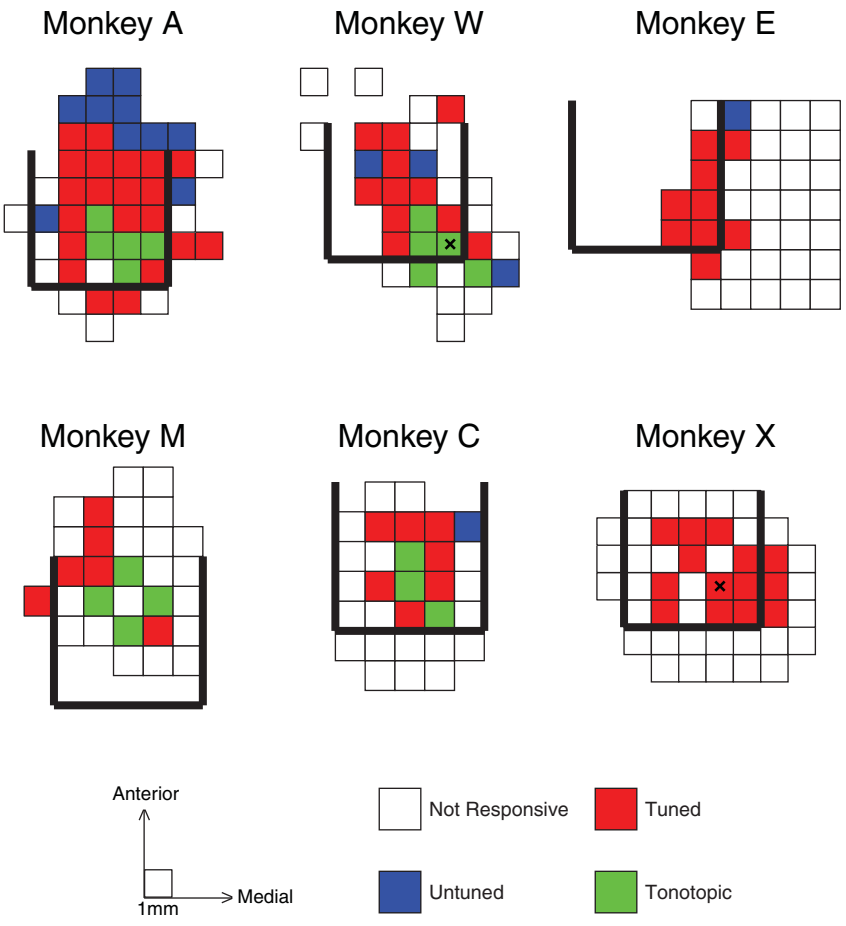
Monkey A
Monkey W
Monkey E
Monkey M
Monkey C
Monkey X
Anterior
Medial
1mm
Not Responsive
Tuned
Untuned
Tonotopic

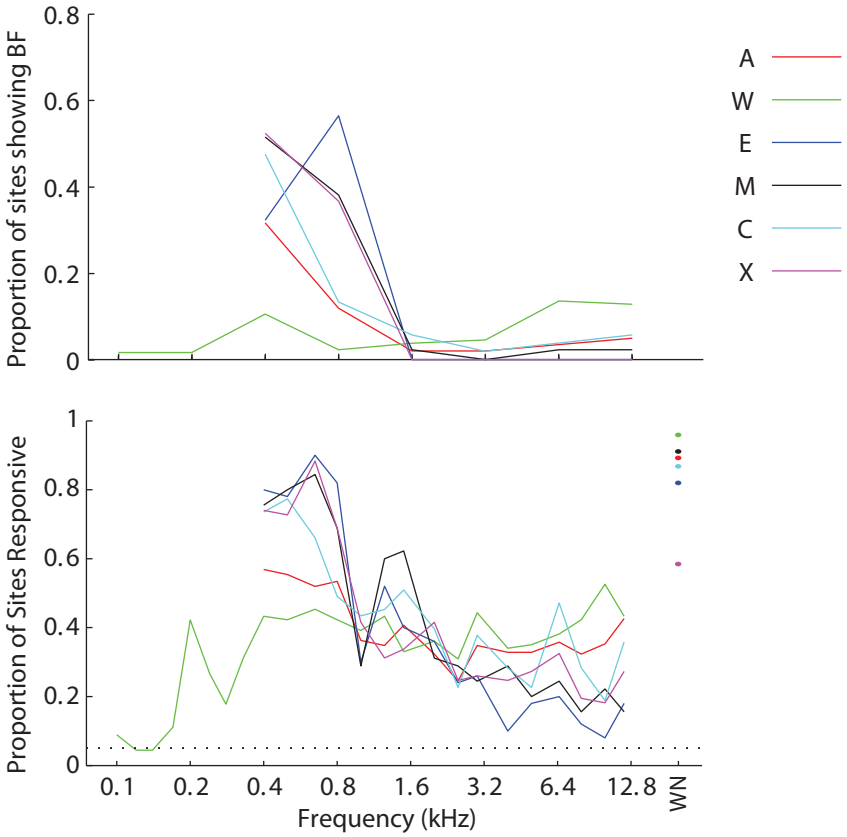
Proportion of sites showing BF
0.8
0.6
0.4
0.2
0
A
W
E
M
C
X
Proportion of Sites Responsive
1
0.8
0.6
0.4
0.2
0
0.1
0.2
0.4
0.8
1.6
3.2
6.4
12.8
WN
Frequency (kHz)

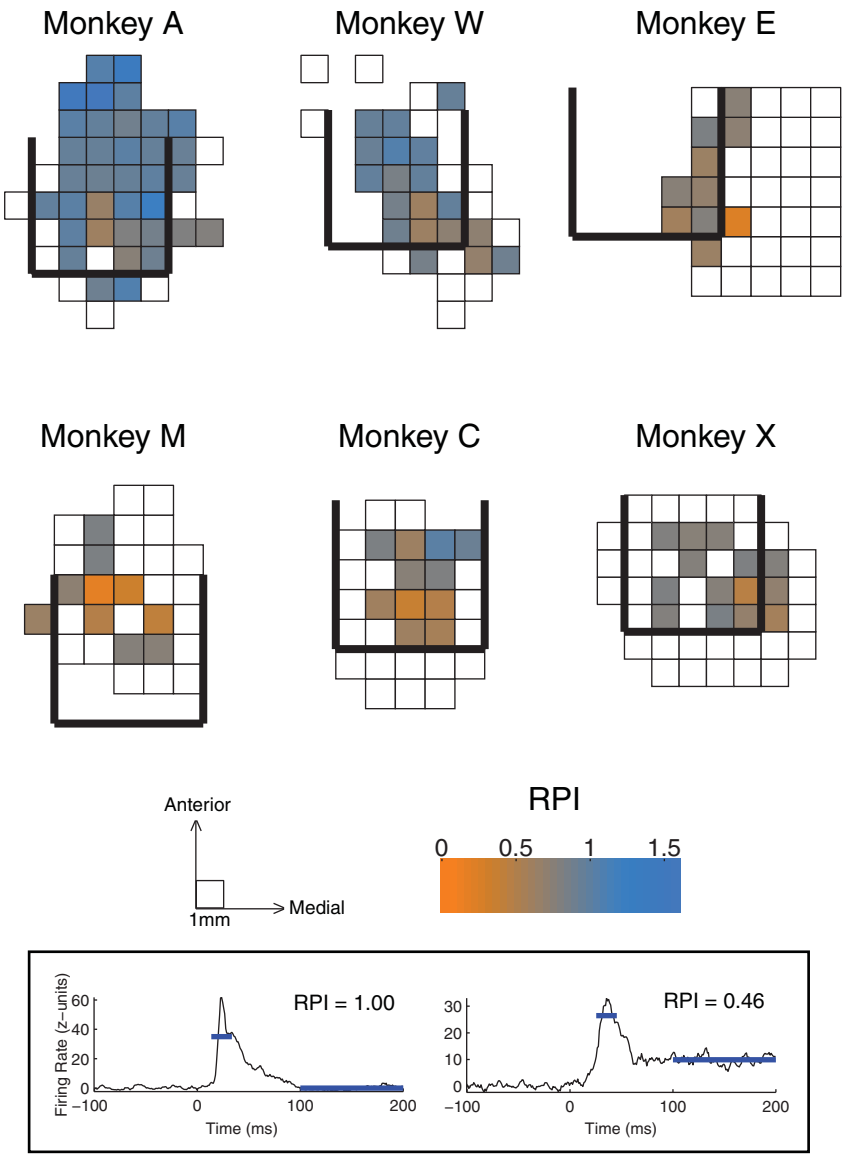
Monkey A
Monkey W
Monkey E
Monkey M
Monkey C
Monkey X
Anterior
Medial
1mm
RPI
0
0.5
1
1.5
RPI = 1.00
RPI = 0.46
Firing Rate (z-units)
Time (ms)
Time (ms)

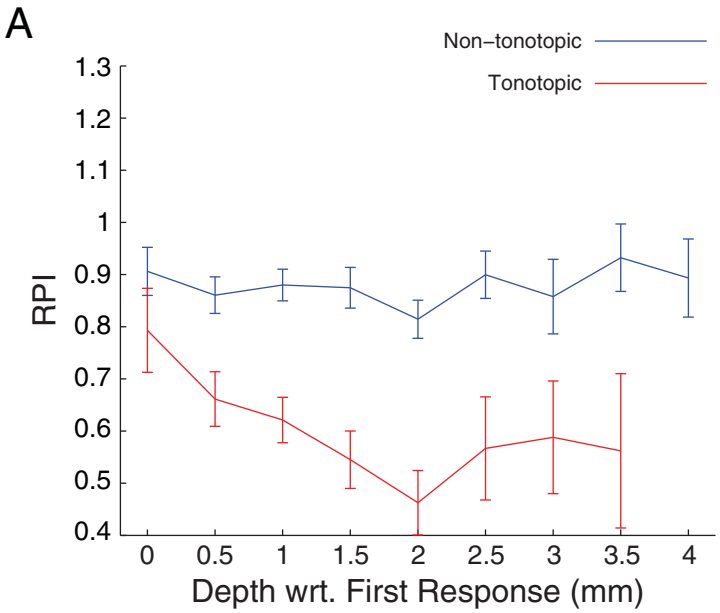
A
Non−tonotopic
Tonotopic
RPI
1.3
1.2
1.1
1
0.9
0.8
0.7
0.6
0.5
0.4
0
0.5
1
1.5
2
2.5
3
3.5
4
Depth wrt. First Response (mm)

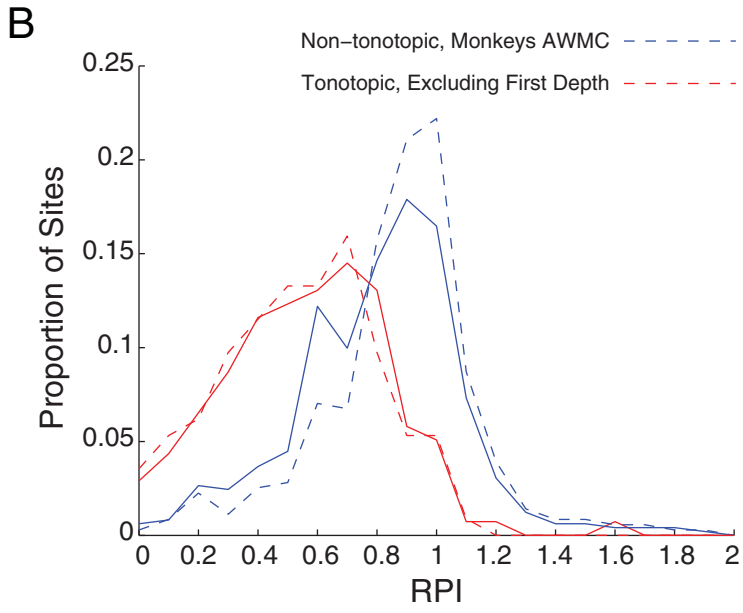
B
Non−tonotopic, Monkeys AWMC
Tonotopic, Excluding First Depth
Proportion of Sites
0.25
0.2
0.15
0.1
0.05
0
0
0.2
0.4
0.6
0.8
1
1.2
1.4
1.6
1.8
2
RPI

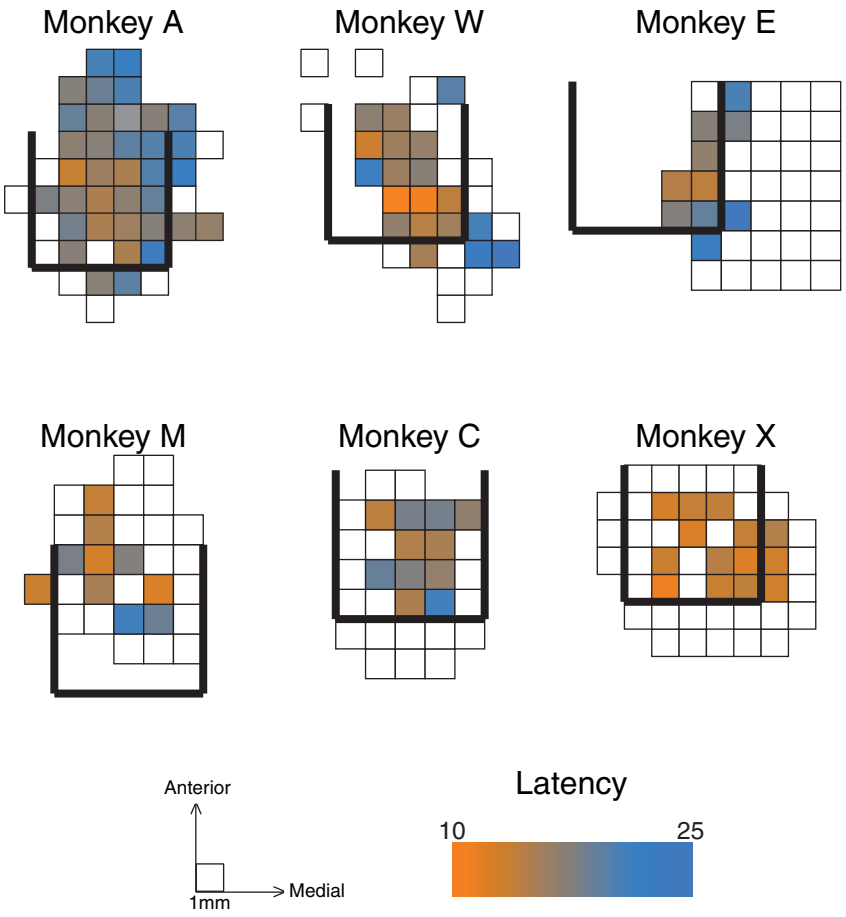
Monkey A
Monkey W
Monkey E
Monkey M
Monkey C
Monkey X
Anterior
Medial
1mm
Latency
10
25

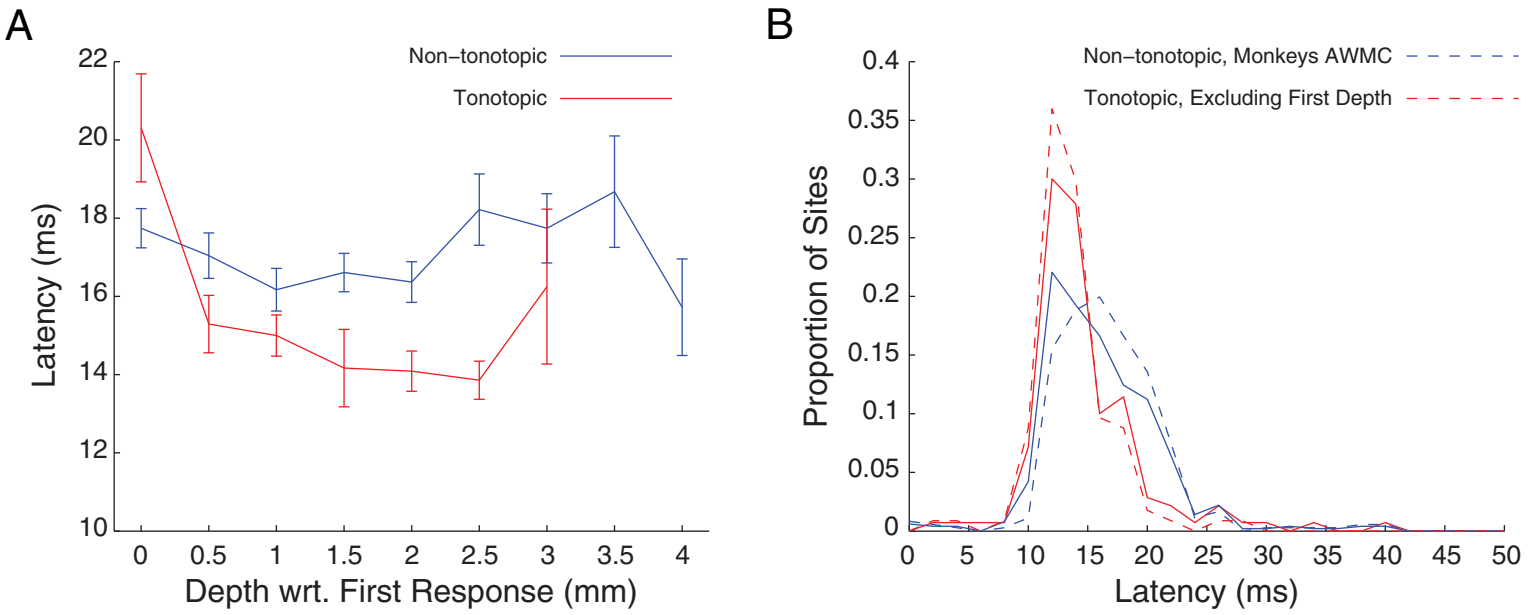
A
Non−tonotopic
Tonotopic
Latency (ms)
Depth wrt. First Response (mm)
22
20
18
16
14
12
10
0
0.5
1
1.5
2
2.5
3
3.5
4
B
Non−tonotopic, Monkeys AWMC
Tonotopic, Excluding First Depth
Proportion of Sites
Latency (ms)
0.4
0.35
0.3
0.25
0.2
0.15
0.1
0.05
0
0
5
10
15
20
25
30
35
40
45
50

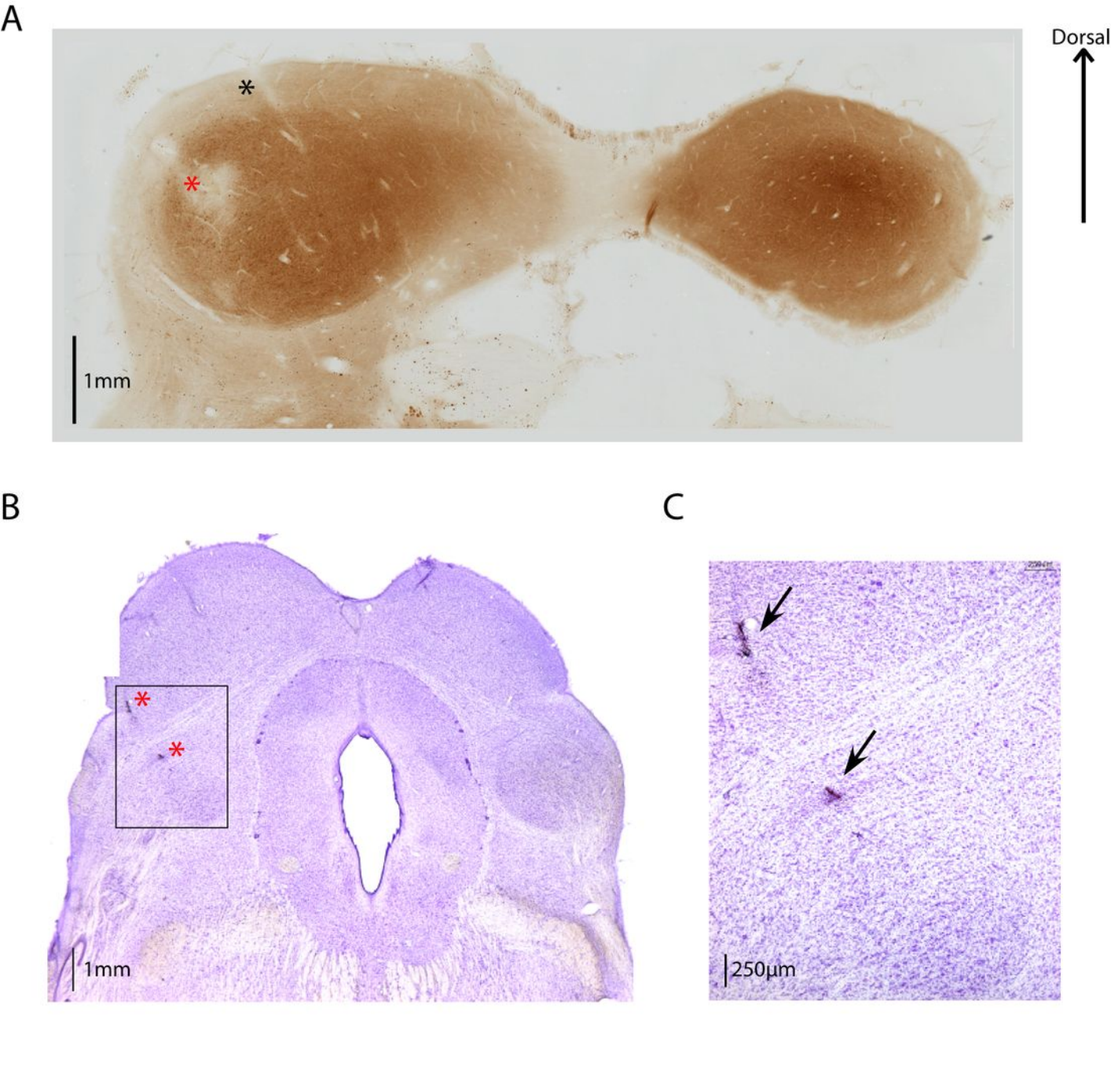
A
Dorsal
1mm
B
1mm
C
250µm

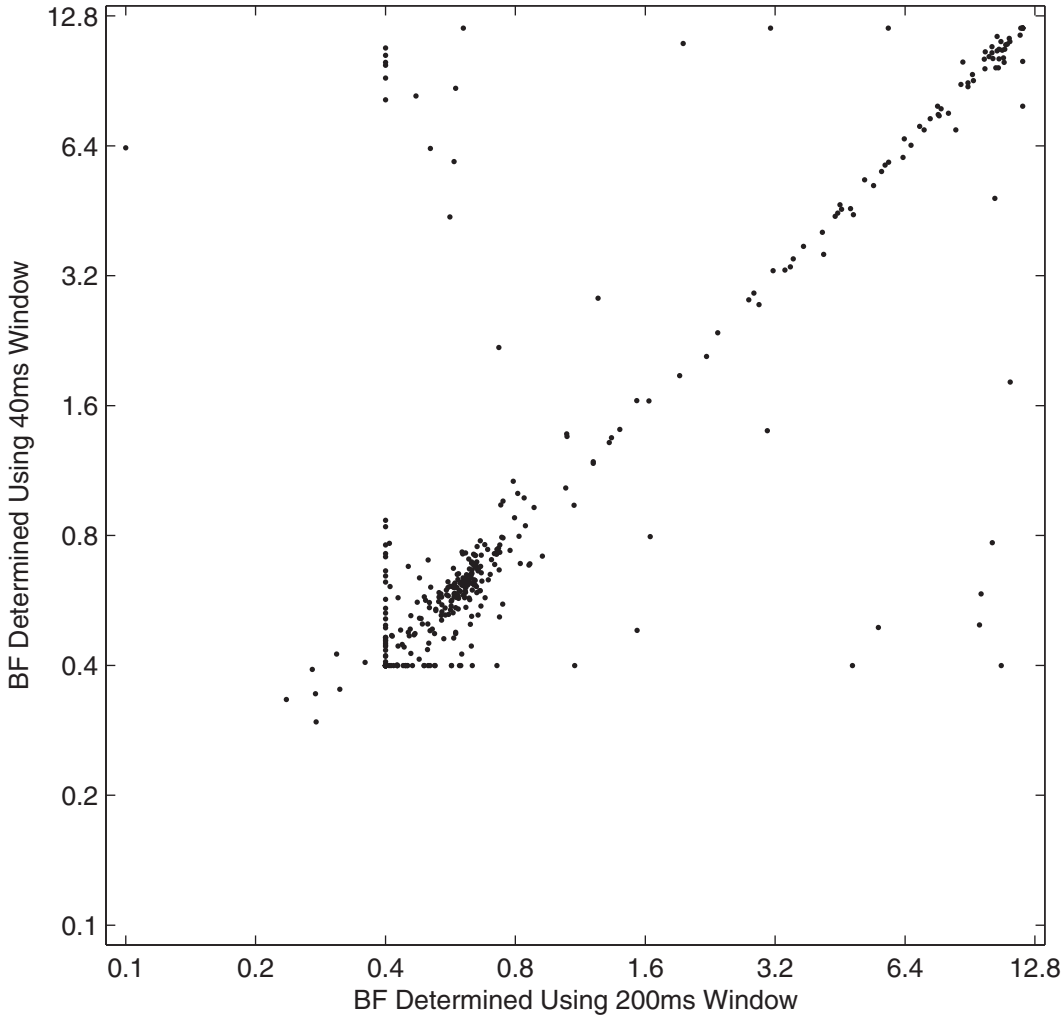
12.8
6.4
3.2
1.6
0.8
0.4
0.2
0.1
BF Determined Using 40ms Window
0.1
0.2
0.4
0.8
1.6
3.2
6.4
12.8
BF Determined Using 200ms Window

Monkey A

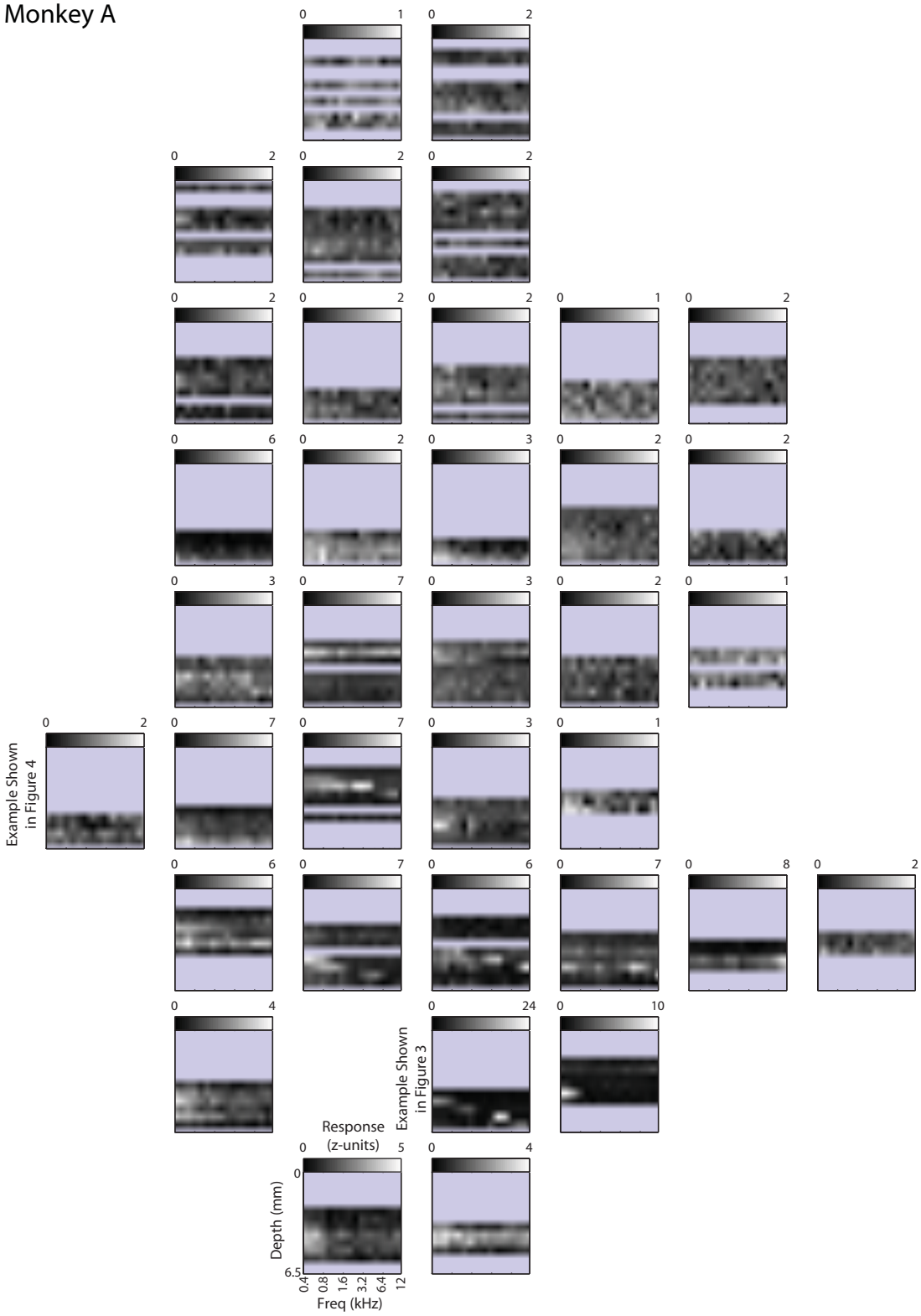
Example Shown in Figure 4
Example Shown in Figure 3
Response (z-units)
Depth (mm)
Freq (kHz)
0.4
0.8
1.6
3.2
6.4
12
6.5

Monkey W

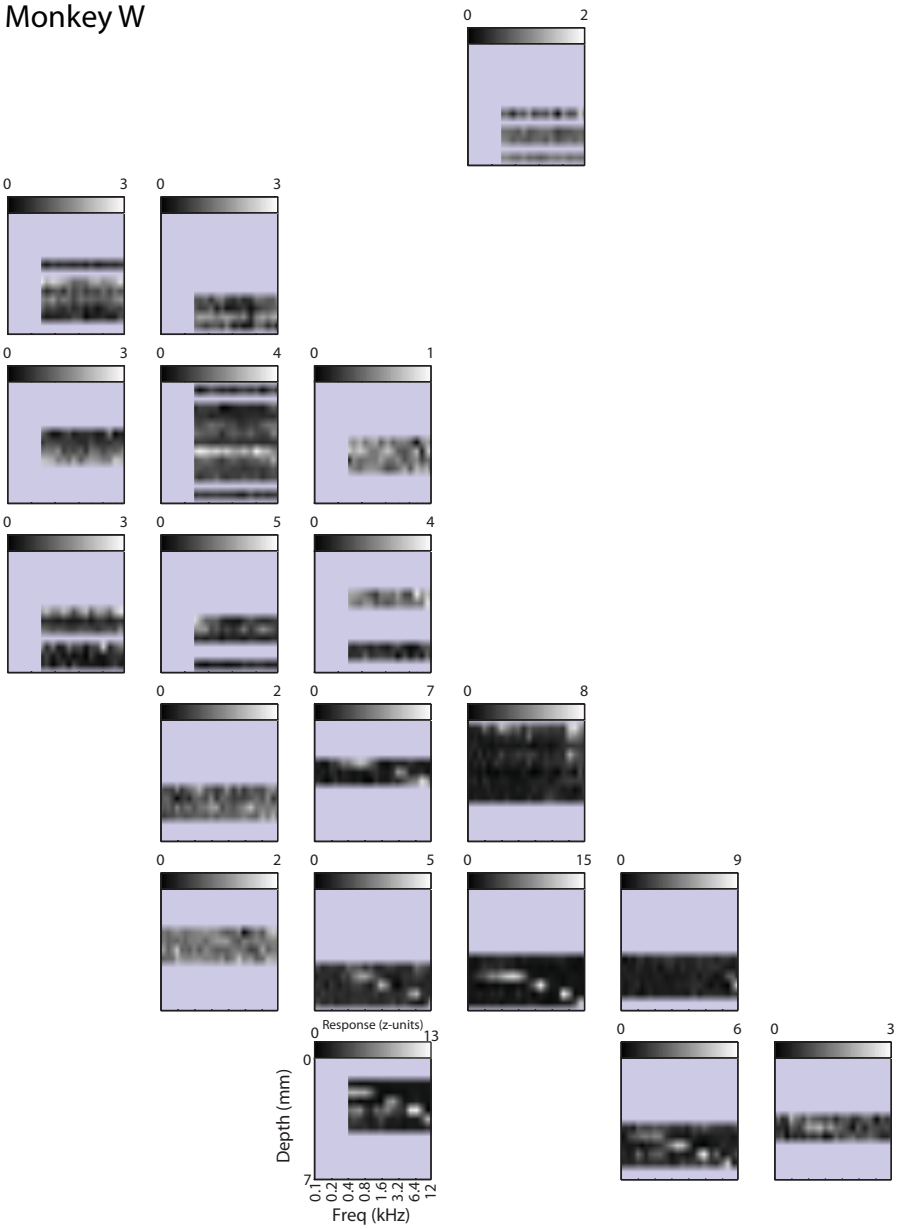
0
2
0
3
0
3
0
3
0
4
0
1
0
3
0
5
0
4
0
2
0
7
0
8
0
2
0
5
0
15
0
9
0
6
0
3
Response (z-units)
0
13
Depth (mm)
0
7
0.1
0.2
0.4
0.8
1.6
3.2
6.4
12
Freq (kHz)

Monkey E

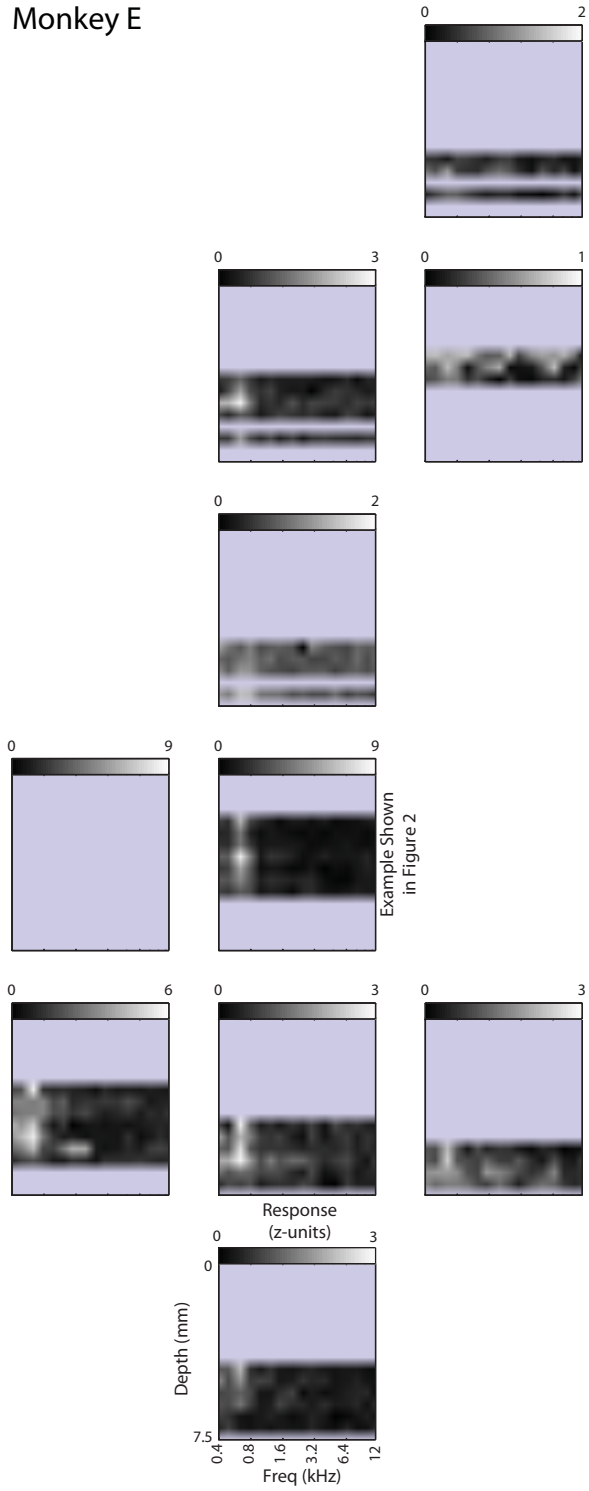
0
2
0
3
0
1
0
2
0
9
0
9
Example Shown
in Figure 2
0
6
0
3
0
3
Response
(z-units)
0
3
0
Depth (mm)
7.5
0.4
0.8
1.6
3.2
6.4
12
Freq (kHz)

Monkey M

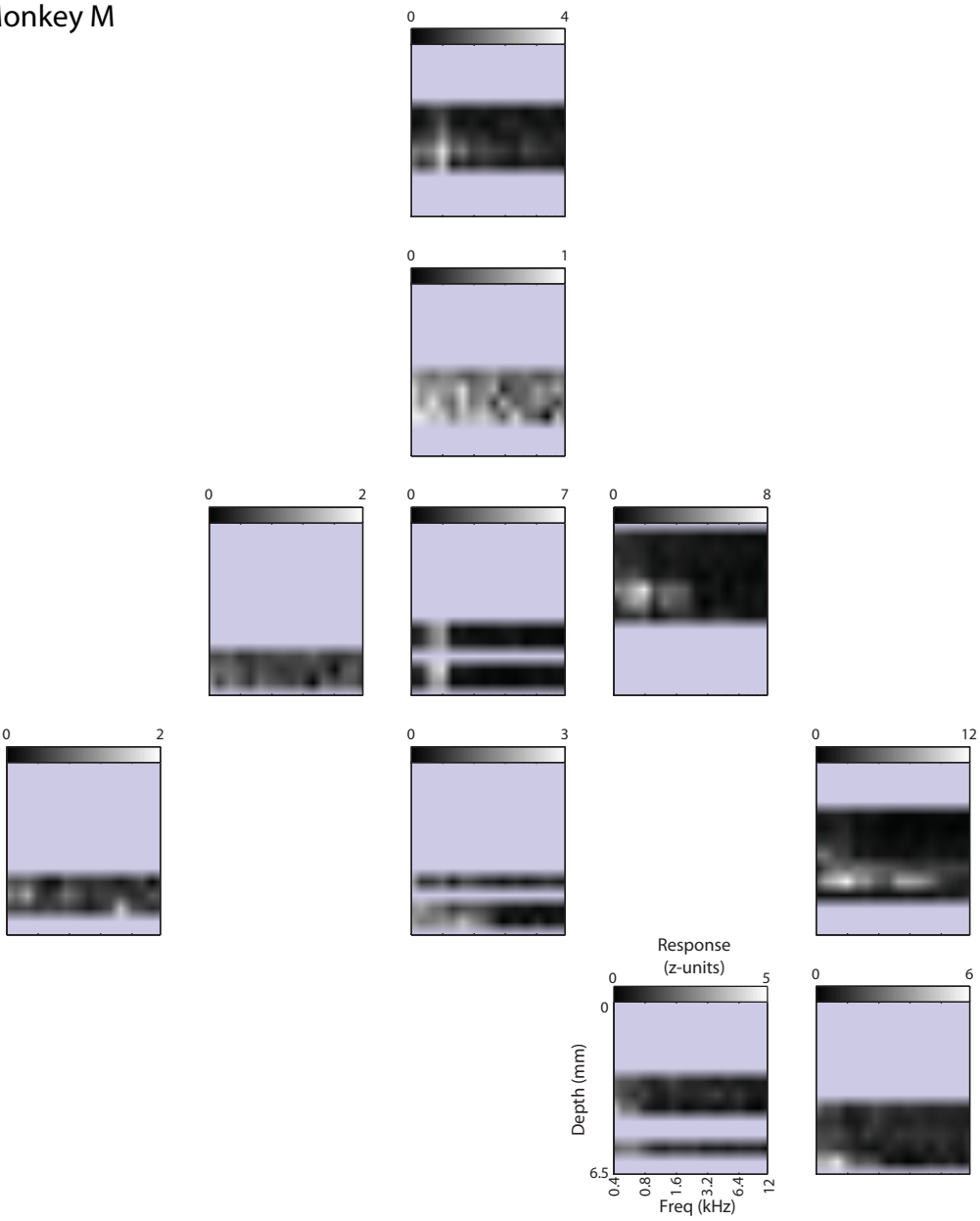
0
4
0
1
0
2
0
7
0
8
0
2
0
3
0
12
Response
(z-units)
0
5
0
6
Depth (mm)
0
6.5
0.4
0.8
1.6
3.2
6.4
12
Freq (kHz)

Monkey C

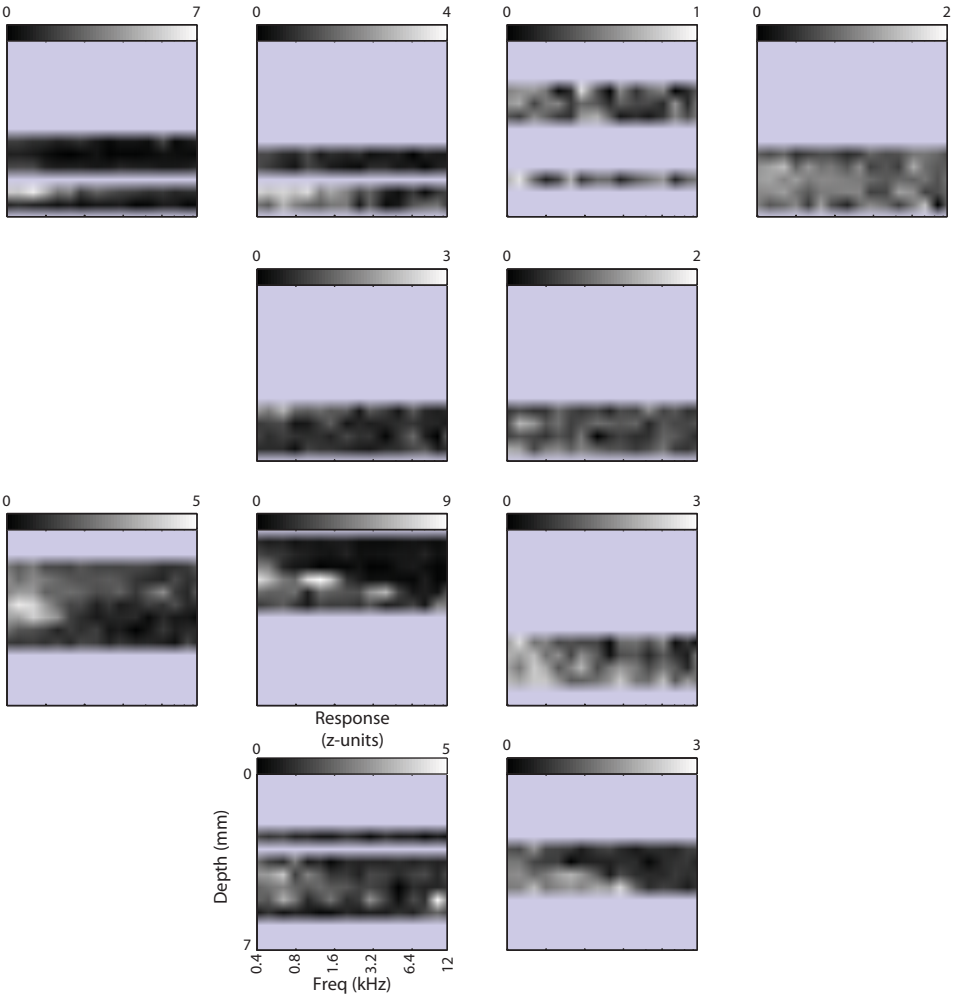
0
7
0
4
0
1
0
2
0
3
0
2
0
5
0
9
0
3
Response
(z-units)
0
5
0
3
0
Depth (mm)
7
0.4
0.8
1.6
3.2
6.4
12
Freq (kHz)

Monkey X

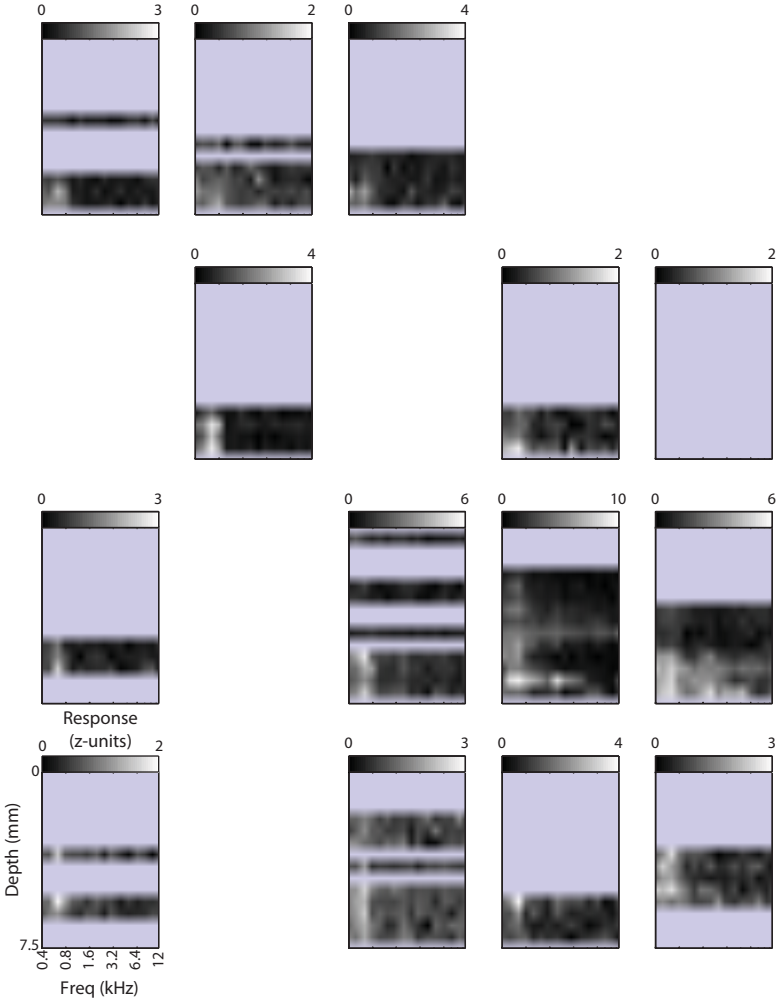
0
3
0
2
0
4
0
4
0
2
0
2
0
3
0
6
0
10
0
6
Response
(z-units)
0
2
0
3
0
4
0
3
Depth (mm)
0
7.5
0.4
0.8
1.6
3.2
6.4
12
Freq (kHz)

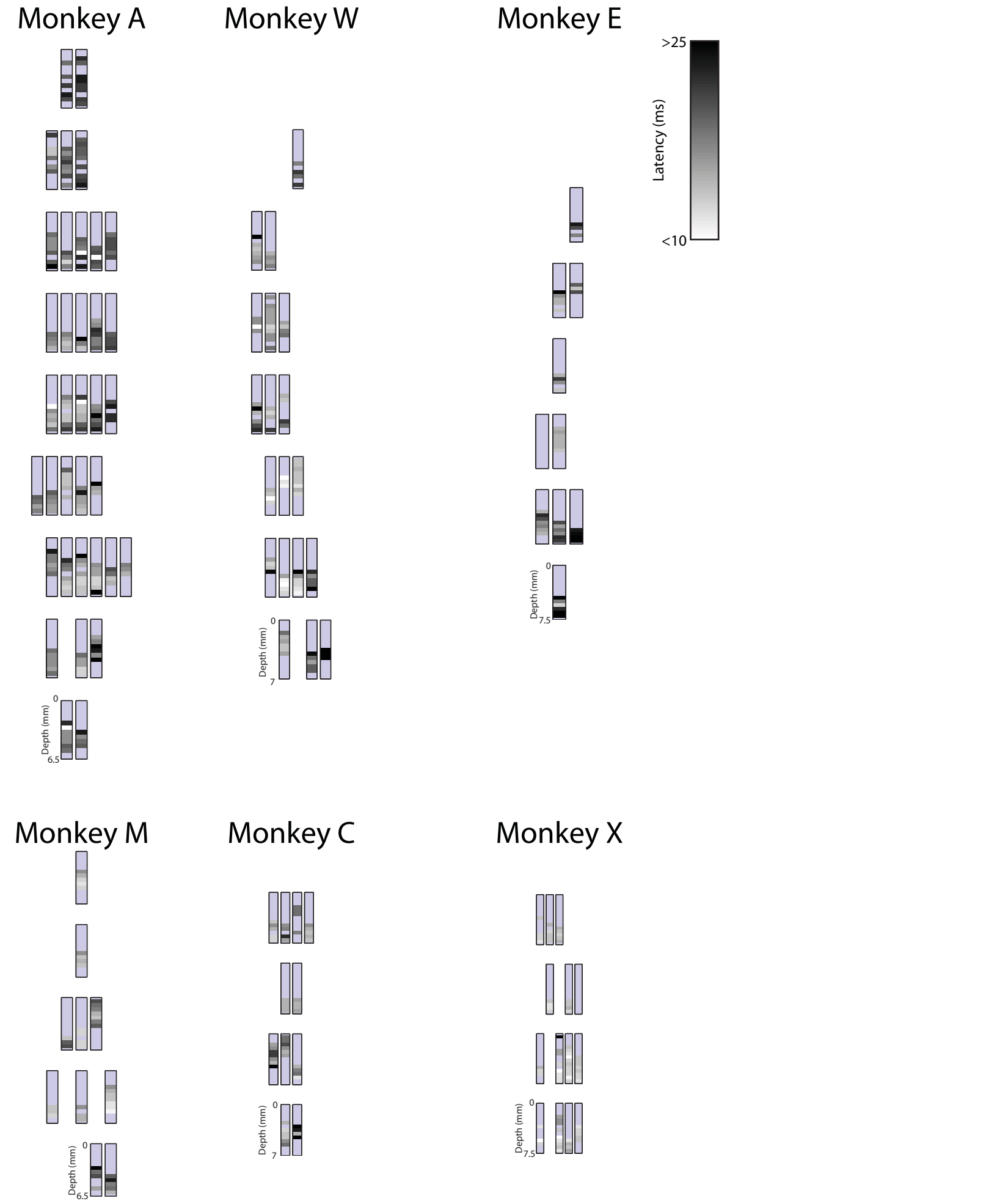
Monkey A
Monkey W
Monkey E
>25
Latency (ms)
<10
Depth (mm)
0
6.5
7
7.5
Monkey M
Monkey C
Monkey X

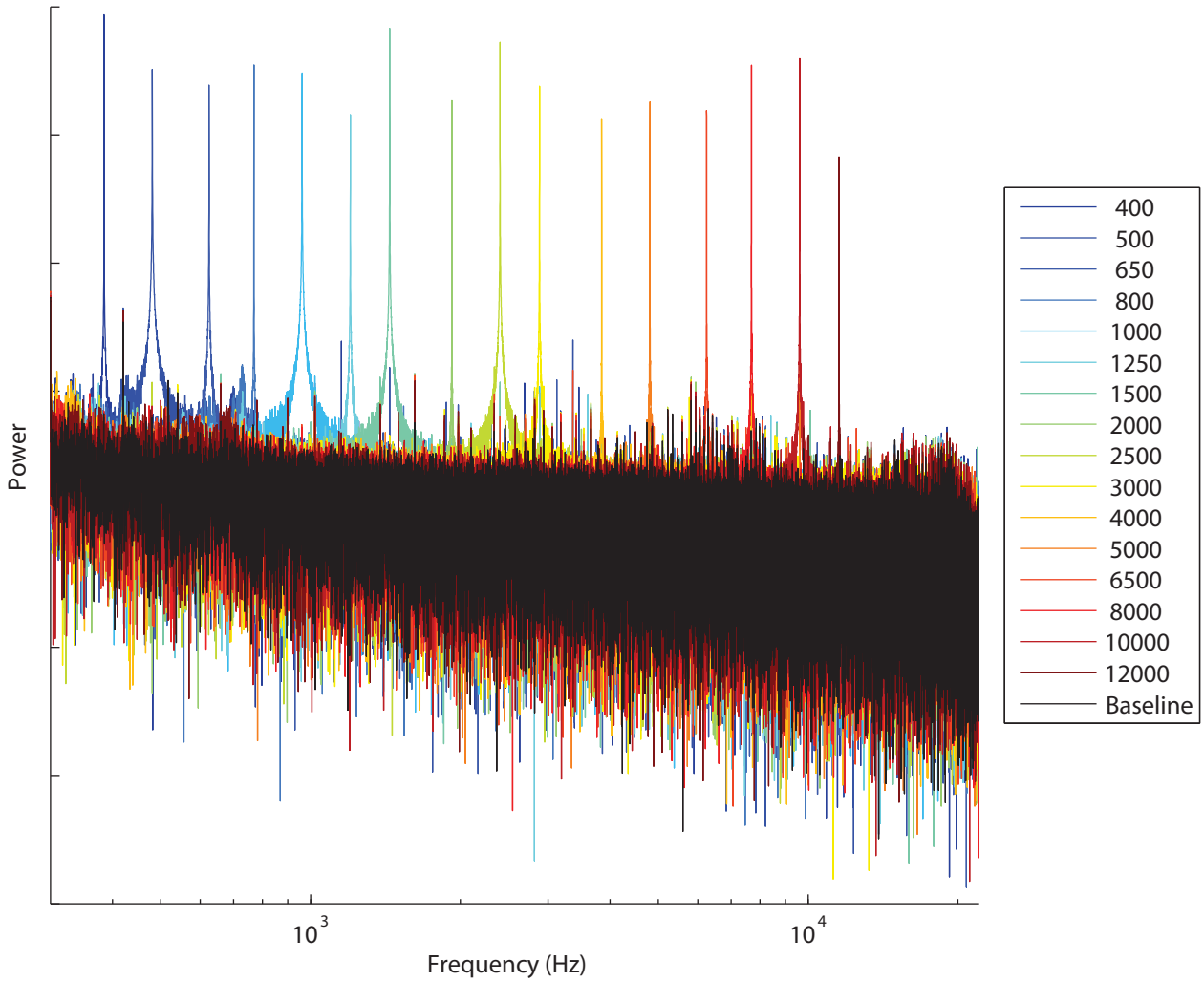
Power
10^3
10^4
Frequency (Hz)
400
500
650
800
1000
1250
1500
2000
2500
3000
4000
5000
6500
8000
10000
12000
Baseline